Winter 1986

SPECTROSCOPIC STUDIES OF THE INTERACTION OF ANIONS WITH TRANSFERRIN (NMR, PYROPHOSPHATE)

SUSAN KEENE SWOPE
University of New Hampshire, Durham

INFORMATION TO USERS

While the most advanced technology has been used to photograph and reproduce this manuscript, the quality of the reproduction is heavily dependent upon the quality of the material submitted. For example:

- Manuscript pages may have indistinct print. In such cases, the best available copy has been filmed.
- Manuscripts may not always be complete. In such cases, a note will indicate that it is not possible to obtain missing pages.
- Copyrighted material may have been removed from the manuscript. In such cases, a note will indicate the deletion.

Oversize materials (e.g., maps, drawings, and charts) are photographed by sectioning the original, beginning at the upper left-hand corner and continuing from left to right in equal sections with small overlaps. Each oversize page is also filmed as one exposure and is available, for an additional charge, as a standard 35mm slide or as a 17"x 23" black and white photographic print.

Most photographs reproduce acceptably on positive microfilm or microfiche but lack the clarity on xerographic copies made from the microfilm. For an additional charge, 35mm slides of 6"x 9" black and white photographic prints are available for any photographs or illustrations that cannot be reproduced satisfactorily by xerography.

Swope, Susan Keene

SPECTROSCOPIC STUDIES OF THE INTERACTION OF ANIONS WITH TRANSFERRIN

University of New Hampshire PH.D. 1986

PLEASE NOTE:

In all cases this material has been filmed in the best possible way from the available copy. Problems encountered with this document have been identified here with a check mark __✓__.

1. Glossy photographs or pages _____
2. Colored illustrations, paper or print _____
3. Photographs with dark background _____
4. Illustrations are poor copy _____
5. Pages with black marks, not original copy _____
6. Print shows through as there is text on both sides of page _____
7. Indistinct, broken or small print on several pages ✓
8. Print exceeds margin requirements _____
9. Tightly bound copy with print lost in spine _____
10. Computer printout pages with indistinct print _____
11. Page(s) _____ lacking when material received, and not available from school or author.
12. Page(s) _____ seem to be missing in numbering only as text follows.
13. Two pages numbered _____. Text follows.
14. Curling and wrinkled pages _____
15. Dissertation contains pages with print at a slant, filmed as received _____
16. Other _____

_____

_____

SPECTROSCOPIC STUDIES OF THE INTERACTION OF ANIONS WITH TRANSFERRIN

BY

SUSAN KEENE SWOPE
BS, Bates College, 1974

A DISSERTATION

Submitted to the University of New Hampshire
in Partial Fulfillment of
the Requirements for the Degree of

Doctor of Philosophy
in
Chemistry

December, 1986

This dissertation has been examined and approved.

N. Dennis Chasteen, Dissertation director
Professor of Chemistry

Christopher F. Bauer
Assistant Professor of Chemistry

C. L. Grant
Professor of Chemistry

Paul R. Jones
Professor of Chemistry

Thomas M. Laue
Assistant Professor of Biochemistry

11/21/86
Date

ACKNOWLEDGEMENTS

I would like to thank the former and present members of my research group for their support, including Ellen Lord, Barbara Viglione, Carl Thompson, Donna Martin and Carmen Valdez (honorary member). I would like to thank John Grady in particular for his assistance in the lab and his role as computer consultant. Finally, my deepest thanks go to Dr. Chasteen for his guidance as my research director. His hard work and kindness in the course of my studies, as well as his dedication and high standards, are greatly appreciated.

DEDICATION

To Greg and Sam

TABLE OF CONTENTS

LIST OF FIGURES

LIST OF TABLES

LIST OF ABBREVIATIONS

bipy	2,2′-bipyridine
EDTA	ethylenediaminetetraacetate
en	ethylenediamine
EPR	electron paramagnetic resonance
Hepes	N-2-hydroxyethyl piperazine-N′-2-ethane sulfonic acid
NTA	nitrilotriacetic acid
PP_i	pyrophosphate
phen	1,10-phenanthroline

ABSTRACT

SPECTROSCOPIC STUDIES OF THE INTERACTION OF ANIONS WITH TRANSFERRIN

by

Susan Keene Swope
University of New Hampshire, December, 1986

Kinetic studies of the uptake of iron by transferrin from iron-pyrophosphate indicate that the reaction proceeds via an intermediate mixed ligand complex of the type PP_i-Fe-transferrin-CO_3^{2-}. The EPR spectrum of the "intermediate" complex was determined by computer modelling of the kinetic data and deconvolution of the experimental spectra. The distinct spectral characteristics of the intermediate indicate that the coordination environment of the iron is different from that of either of the reactants, consistent with formation of a complex in which iron is coordinated to both transferrin and pyrophosphate.

Studies of the interaction of sodium cyanide with iron(III)-transferrin demonstrate that a low-spin cyanide adduct of transferrin is produced which exhibits a rhombic EPR spectrum with principal components at $g' = 1.92$, 2.15 and 2.34. The stoichiometry of adduct formation is:

$$Fe_c\text{-Tf-}HCO_3 + 3\ CN^- \longrightarrow Fe_c\text{-Tf-}(CN)_3 + HCO_3^-$$

where adduct formation only occurs at the C-terminal domain and the subscript "c" designates this half of the protein.

This is the first example of an inorganic anion substituting for bicarbonate in transferrin. The results also show that ligands in the first coordination sphere of iron bound at the specific iron binding site in transferrin are susceptible to displacement by chelators in solution.

Nitrate binding to transferrin was studied using N-15 paramagnetic relaxation enhancement. Significant relaxation enhancement of the N-15 nucleus in the presence of bound paramagnetic iron was observed, indicating that the anion binding site is close to the metal on the protein. The metal anion distance was estimated to be in the range of eight to fifteen Angstroms.

INTRODUCTION

Iron and Transferrin

Iron is the most abundant transition metal in the earth's crust (1), and is a component of almost every known living organism (2). The human body contains approximately four grams of iron in both the ferrous and ferric oxidation states (3). In aqueous solution at physiological pH, the ferrous ion is readily oxidized by molecular oxygen. Ferric ion at neutral pH forms insoluble hydroxides; K_{sp} for ferric hydroxide is 6×10^{-38} (1). Therefore, given the high requirement for iron, and its low bioavailability, humans and other higher organisms have developed specialized proteins for sequestering and transporting iron.

The transferrins are a class of metal-binding proteins capable of strongly binding two atoms of Fe(III) with an apparent stability constant of the order of 10^{24} (3). Besides serum transferrin, the two other major transferrins are ovotransferrin, from egg white, and lactotransferrin, from milk. The transferrins have a molecular weight of approximately 80,000, and each molecule consists of two homologous halves or "domains" containing one iron binding site. The iron binding sites are similar, but not identical. Serum transferrin, subsequently referred to simply as transferrin, is the circulatory iron transport protein of the circulation. The primary function of lactotransferrin may be both nutritional and antibacterial, respectively increasing the bioavailability of iron in the gastrointentinal tract and limiting the availability of iron

needed for microbial growth. Ovotransferrin may have an analagous purpose in the developing egg (4).

The general scheme for iron uptake from transferrin has been established on the cellular level. Cells which require iron have specific transferrin receptors located on the outside of the cell. The iron-transferrin complex is internalized from serum into the cell by receptor-mediated endocytosis: transferrin loaded with iron has a high affinity for the transferrin receptor. Once bound, the transferrin-receptor complex is internalized, and makes its way to an acidic compartment within the cell. In this low pH environment, protonation of groups at or near the iron-binding site presumably destabilizes the iron-protein complex and facilitates iron removal, possibly by intracellular chelating agents. Once the transferrin-receptor complex returns to a neutral pH, the apotransferrin loses its affinity for the receptor and is released to the extracellular environment (5). This scheme is consistent with the fact that transferrin is conserved during iron delivery; the half life of iron and transferrin in serum is 1-2 hours and 8 days respectively (6).

The Structure of Transferrin

Definitive structural determinations of proteins generally require both a complete amino acid sequence and an x-ray crystal structure. The amino acid sequence gives the primary structure of the protein, while x-ray data can be

used to determine its tertiary structure, i.e. conformational aspects of the structure. The amino acid sequences of human serum transferrin (7), human lactotransferrin (8), and hen ovotransferrin (9,10) have all been solved within the past few years. The most remarkable feature of the primary structure is that of definite homology between the two "halves" of the protein; *homologous proteins are proteins assumed to be derived from a common anscestor due to significant similarities in their structure.* For human serum transferrin, the two homologous halves consist of residues 1-336 and 337-678, in which 40% of the residues are identical (7).

Because of the weak diffraction pattern of transferrin, determination of a high resolution x-ray structure has not been successful (11). However, a low resolution map has been acquired which clearly shows the two globular "domains" of transferrin, each containing an iron binding site; the approximate maximum dimensions of the protein are 9.5 x 6.0 x 5.0 nm (12).

Prior to determination of the amino acid sequence, evidence from spectroscopic, chemical modification, and equilibrium studies suggested that the amino acids serving as ligands at the iron binding site were two histidines, two or three tyrosines, and either an arginine or histidine bridged by carbonate or bicarbonate. The first coordination sphere of the bound metal also likely contains either water or hydroxide, giving a six- or seven-coordinate iron binding site (13).

Publication of the complete amino acid sequence of three transferrins has provided enough information to predict the specific amino acids involved in iron binding. Because all transferrins bind iron in a similar fashion, and since evidence suggests that iron binding is the primary function of transferrin, it is reasonable to assume that the amino acids serving as ligands for iron would be conserved over the course of evolution. Consequently, it has been possible to specify the likely location for the amino acids involved in iron binding (13,14).

Chasteen has constructed a string model based on the likely disulfide bridges formed from cysteine residues. This model shows a concentration of positively charged amino acids in the region of the iron binding site (13). Apart from the amino acids which are likely candidates for ligands, one histidine, two arginines, and two or three lysines in each domain are also conserved and expected to be in the iron binding region.

Unique Properties of Transferrin

Much of the research in transferrin chemistry has been prompted by the interesting properties of the protein. Many questions concerning these properties remain: Are there significant differences in the two iron binding sites? If so, do the two sites function differently in vivo? What is the detailed mechanism by which transferrin with such a high affinity for iron can release it so readily when required?

What is the role of anions in the uptake and release of iron by transferrin?

Given that transferrin has two iron binding sites, a logical question involves establishing the differences between the iron binding sites, particularly with respect to functionality. In general, the two sites are very similar, and there is no conclusive evidence that the sites function differently in vivo. It may be, as Williams has suggested (15), that the transferrin molecule has been doubled in size during the course of evolution in order to preclude excretion of the protein from the serum by glomerular filtration. The fact that the transferrin molecule has two iron binding sites could then be interpreted as being just a fortuitous result of the doubling of the singly sited protein.

However, iron is not randomly distributed between the N-terminal and C-terminal sites of transferrin in serum. Leibman and Aisen (16) reported the average distribution of iron in transferrin in normal serum is 37% apotransferrin, 7% C-terminal transferrin, 45% N-terminal transferrin, and 11% diferric transferrin. Zak and Aisen argue that, given this fact, there necessarily are functional differences between the two sites. They suggest the possibility of a correlation between the relative distribution of iron in the C- and N-sites and overall serum iron levels; individuals with low overall serum iron levels tended toward preferential distribution of iron in the more strongly binding C-terminal site, while the population generally

showed preferential binding at the thermodynamically less stable N-terminal site (17).

Although the ligands at both the N- and C- terminal sites are generally believed to be the same, the overall environments of the two sites are dissimilar enough to reveal some spectroscopic and kinetic differences. A differential pH effect on the N-site versus the C-site was first reported by Princiotto and Zapolski in 1975 (18). They showed that transferrin which was more than half saturated with iron lost its iron in two steps as the pH was lowered; iron was lost from one site at a pH of approximately 5.7, but was not lost from the other site until the pH was lowered to approximately 5.0. They also demonstrated that this differential pH sensitivity could be used to bind iron selectively at the acid-stable site (the C-terminal site).

In 1976 Makey and Seal (19) developed an electrophoresis method for separation of the four forms of transferrin: apotransferrin, C-terminal monoferric transferrin, N-terminal monoferric transferrin and diferric transferrin. This method provided for the first time a means of measuring the iron distribution in samples of partially iron-saturated protein.

In 1980, Williams and Moreton (20) showed that the distribution of iron between the N- and C- terminal sites was dramatically affected by dialysis. This was shown to be due to the presence of low molecular weight components,

principally NaCl, which increase the stability of the N-terminal site relative to the C-terminal site (21). Salts also retard the rate of iron removal from the N-terminal site but increase the rate of removal from the C-terminal site (22). Although most salts have an influence, some are more effective than others in promoting these site-specific changes. Perchlorate has a particularly pronounced influence on the protein; the relative stability of the N-site compared to the C-site is increased 17-fold in the presence of 0.5 M $NaClO_4$ at pH 7.4 (21). Perchlorate is known to have a particularly high affinity for positively charged groups on proteins (23).

Spectroscopic Properties

Apotransferrin has an intense absorption band in the UV centered at 280 nm, characteristic of most proteins (ϵ = 9.23 X 10^4 $M^{-1}cm^{-1}$ (24). This band results from π to π^* transitions of the aromatic amino acids (tryptophan, tyrosine, and phenylalanine). Binding of iron to apotransferrin increases the intensity of UV absorption at 295 and 245 nm (25), as shown by the difference spectra. The visible absorption spectrum of iron transferrin consists of a band centered at 465 nm (ϵ = 2500 $M^{-1}cm^{-1}$ per Fe) (26). Model studies with iron phenolates indicate that the transition is due to a charge transfer band from the phenolate oxygen of tyrosine to the metal (27).

Along with the UV-vis absorption spectra, EPR spectroscopy has been widely used for the study of

transferrin. Because EPR is sensitive only to the presence of unpaired electrons, it is well-suited for study of the binding site of the paramagnetic iron. The X-band EPR spectrum of iron bound to transferrin is characeristic of the protein: "no other iron containing protein displays such a signal, no model compound has ever been prepared which reproduces it, and it has never been adequately simulated" (28).

The EPR spectrum of transferrin arises from transitions within the Kramer's doublets. Kramer's theorem states that, at zero field, the angular momentum states of a system with an odd number of unpaired electrons will occur in pairs. Consequently, high-spin iron, with five unpaired electrons, has three pairs of Kramer's doublets. In an applied field, the degeneracy of these states is removed (see Fig. 1).

The X-band EPR spectra of high spin iron in rhombic fields is characterized by resonances centered at $g' = 4.3$ and $g' = 9.7$ ($g' = h\nu/\beta H_{obs}$), arising from transitions within the middle Kramer's doublet, and both the upper and lower Kramer's doublet, respectively (29). For iron transferrin, the characteristic portion of the spectrum is resolved into 3 components and centered at $g' = 4.3$. A much less intense band is also observed at $g' = 9.7$ (see Fig. 2).

The EPR spectrum of transferrin is dramatically affected by ligand substitution at the metal site. It is also sensitive to changes in the vicinity of the iron binding region, presumably because of the effect these

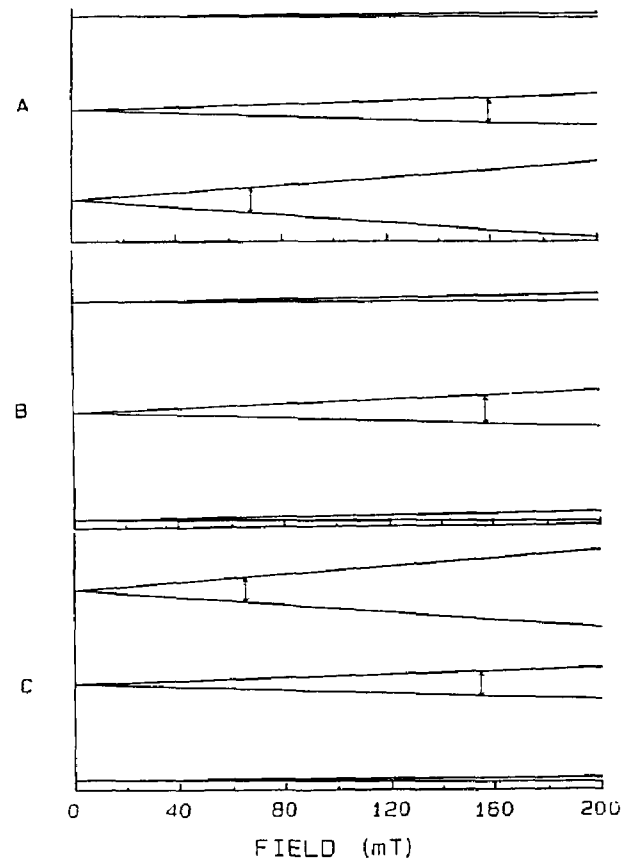

Figure I-1. Splitting of the Kramer's doublets in transferrin in the presence an an applied field at various orientations. A, B and C are for the magnetic field parallel to the x, y and z axes of the g-tensor, respectively. Vertical arrows indicate transitions at X-band frequencies. Adapted from reference 29.

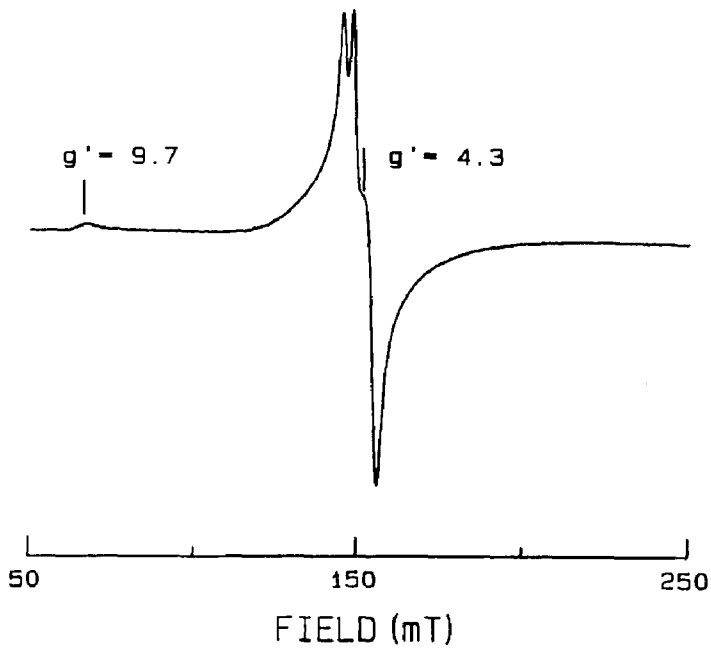

Figure I-2. X-band EPR spectrum of diferric human serum transferrin at 77 K. The lines around 150 milliTesla arise from transitions within the middle Kramer's doublet; the weaker signal near 70 milliTesla arises from transitions from the upper and lower Kramer's doublet. (See Fig. 1). Instrument parameters: Modulation amplitude = 0.5 milliTesla, microwave power = 5 milliwatts, receiver gain = 1000, scan time = 16 min/200 milliTesla, microwave frequency = 9.149 GHz, time constant = 1 s. Solution conditions: 0.426 mM protein, 10 mM Hepes, 25 mM sodium bicarbonate, pH 7.5. File FE2TF.2K, Disc #8, JG.

changes have on ligand orientation about the metal. EPR spectroscopy has proven to be a fruitful approach to the study of anion-protein interactions. However, a detailed analysis of the $g' = 4.3$ signal in iron(III) EPR signals in relation to the metal site is not yet available (28).

Anion Binding to Transferrin

Transferrin cannot bind iron at the specific iron binding site in the absence of a synergistic anion, which is normally bicarbonate. Although other anions can be substituted for bicarbonate, for example malonate and oxalate, they are readily displaced in the presence of bicarbonate. The synergistic anion binds directly to the iron, most likely bridging the region between the metal and a positively charged amino acid. Both the optical and EPR spectra are dramatically changed by the replacement of bicarbonate as the synergistic anion (30,31).

In 1972 Price and Gibson (32) first noted the effects of salt (specifically perchlorate) on the EPR spectrum. The fact that perchlorate produced a loss of resolution and a decrease in the amplitude of the $g' = 4.3$ signal led them to speculate that perchlorate caused a conformational change in the protein.

More recently, Folajtar and Chasteen have studied perturbations of the EPR spectra of transferrin in the presence of various salts as a function of concentration (33). Detailed thermodynamic analysis of these results showed that there are two anion binding sites in each domain

of diferric transferrin. The anions thiocyanate, perchlorate, and pyrophosphate were shown to bind most strongly. Subsequent chemical modification studies have correlated specific amino acids such as lysine with differential effects on the EPR spectra of the N-terminal versus C-terminal site (34). These results are consistent with the hypothesis that there are specific anion-binding sites on the protein which function to modulate the uptake and release of iron from transferrin.

The following work described in this thesis is an attempt to gain more understanding of the chemistry of transferrin, particularly with respect to the function of anions in the iron binding properties of the protein. Ultimately, the goal of this kind of research is to understand in detail the relationship between the structure of transferrin and the mechanism by which this protein exchanges iron with its environment.

CHAPTER I

CHARACTERIZATION OF AN INTERMEDIATE IN THE EXCHANGE OF IRON(III) BETWEEN PYROPHOSPHATE AND TRANSFERRIN

INTRODUCTION

In spite of the large amount of research on the chemistry of transferrin, the sequence of steps leading to formation of the Fe^{3+}-transferrin-CO_3^{2-} complex from iron and bicarbonate is not known (4). The insolubility of unchelated iron(III) at physiological pH suggests that mixed ligand complexes of the type chelator-Fe^{3+}-transferrin-CO_3^{2-} are probably formed as intermediates in the exchange of iron between transferrin and chelators (35). However, it was not until 1982 that Cowart et al. provided the first spectroscopic evidence for formation of an intermediate in the reaction of apotransferrin and iron(III) aceto-hydroxamate (AHA) (36).

Detailed kinetic studies of this reaction led to the proposal of a generalized scheme for iron uptake by transferrin. Features of the proposed five-step mechanism include labilization of the iron chelate complex followed by combination with the binary apotransferrin-CO_3^{2-} complex to form the intermediate complex. In order to test the hypothesis for a common reaction route for iron addition, further work was done using the chelator pyrophosphate (37).

Pyrophosphate, a ligand which has a possible cellular iron transport role, has also been shown to be the most effective chelator in increasing the rate of iron removal from transferrin (38,39). Visible absorption spectroscopy has provided evidence for formation of an intermediate during

the delivery of iron to transferrin by pyrophosphate (37). In the following study, EPR spectroscopy was used in an attempt to detect and further characterize this intermediate. Compared to absorption spectroscopy, EPR spectroscopy is often more sensitive to the ligand environment of a metal. However, it is more difficult to obtain EPR kinetic data since frozen solutions are required for EPR measurements of Fe(III). Quantitation of EPR intensity data is more difficult as well. We found it useful to couple the results of absorption and EPR measurements in our present investigation.

MATERIALS AND METHODS

All reagents were reagent grade and used without further purification. Iron-free human serum transferrin of stated 98% purity was obtained from Calbiochem-Behring and dialyzed first against three changes of 0.15 M sodium perchlorate and 0.002 M Hepes, pH 6.8, and then against three changes of 0.002 M Hepes, pH 6.8. Determination of apotransferrin concentration was based on the absorptivity $\epsilon^{1\%}_{1cm}$ = 11.4 at 280 nm and a molecular weight of 78,000. Apotransferrin was prepared at a concentration of (4-6) x 10^{-4} iron-binding equivalents/liter in 0.1 M Hepes and 20 mM $NaHCO_3$ at pH 7.4.

Fe^{3+}-pyrophosphate was prepared in a 3.7:1 PP_i:Fe ratio and a final concentration of 0.3 mM Fe^{3+} by the addition of $Fe(NH_4)_2(SO_4)_2$ (Baker) in 0.01 M HCl to pyrophosphate

(tetrasodium pyrophosphate, decahydrate, Aldrich) in 0.1 M Hepes, 20 mM $NaHCO_3$, pH 7.4, at 0°C followed by air oxidation of the iron. Completion of the oxidation process in 5-10 min was verified by monitoring the amplitude of the g' = 4.3 EPR signal of the Fe^{3+}-pyrophosphate signal.

In order to retard the rate of the reaction of Fe^{3+}-pyrophosphate with apotransferrin, the solutions and reaction mixture were maintained in an ice bath. Sufficient Fe^{3+}-pyrophosphate was added to apotransferrin-CO_3^{2-} to 50% saturate the protein. The reaction was monitored spectrophotometrically at either 245 or 465 nm in a compartment of a Cary 219 spectrometer thermostatted at 0°C. At selected intervals aliquots of the reaction mixture were removed, placed in a quartz EPR tube, and quickly frozen in a dry ice-acetone bath or in a pentane slush. The freezing time of the reaction mixture was determined with a copper-constantan thermocouple in the EPR tube. From the time elapsed between tube immersion and the rapid rise in temperature following supercooling of the sample the freezing time was determined to be approximately 5 s. A stopped flow apparatus was used to obtain the spectrum of the Fe^{3+}-pyrophosphate in the presence of apotransferrin prior to reaction with the protein. After rapid mixing of the reactants in the upstream portion of the apparatus, the mixture was discharged as a fine spray into a flared top EPR tube containing liquid pentane at -75°C. The residence time of the reactants prior to freezing was estimated to be 1.3 s. The fine ice crystals were firmly tamped into the bottom

of the EPR tube with a glass rod. The EPR spectrum showed no evidence of reaction of the iron pyrophosphate with the protein and was the same as that in the absence of protein.

EPR spectra were measured at X-band (9.1 GHz) frequency with Varian E-4 and E-9 spectrometers interfaced to a MINC-23 computer. The temperature was maintained at 77 K with a liquid nitrogen Dewar flask and a split plastic straw insert in the Dewar tip to minimize instrument noise from liquid nitrogen bubbling. EPR tubes were calibrated to one another using an iron pyrophosphate solution. To evaluate EPR intensities, double integrations of first-derivative spectra were calculated between the limits of 55 and 220 mT.

Urea polyacrylamide gel electrophoresis was used to determine the distribution of iron between the two sites following 50% saturation of the protein. Samples from the EPR kinetic study were quickly thawed one at a time and immediately diluted in tank buffer/glycerol solution, pH 8.4, and loaded onto the gel. The sample was electrophoresed at 400 V for 5 min until the tracking dye had migrated into the gel after which time the next sample was thawed and loaded. Final electrophoresis was done at 120 V. The Coomassie Blue R-250 stained gels were scanned with a Hoeffer Scientific densitometer interfaced to the MINC-23 computer for determination of the area under the peaks.

RESULTS

In the initial stages of this project, we obtained EPR spectroscopic evidence for formation of an intermediate in the reaction between iron(III)-pyrophosphate and apotransferrin. This work was part of a collaborative study with Dr. George Bates and co-workers at Texas A & M University. The Bates group had previously obtained evidence for an intermediate from room temperature visible absorption spectroscopy with a rapid scan spectrophotometer. An independent confirmation of this finding was needed. Their work suggested a mechanism in which the intermediate was formed in a fast first step, followed by first-order decay to product.

However, the observed decay to product did not rigorously follow first-order kinetics, particularly at lower temperatures. Furthermore, it was not possible to simulate their data by assuming a second-order formation of intermediate followed by simple first order-decay to product. Thus, the reaction was complex and other likely possibilities had to be considered, including (a) the presence of polymeric iron species in solution and (b) the question of kinetic heterogeneity associated with addition of iron to the N- and C-terminal iron binding sites of the protein. These possibilities will be addressed in the following two sections of this chapter.

Effect of Solution Conditions on the Homogeneity of the Fe(III)-PPi Complex as Determined by EPR

The EPR signal intensity is indicative of the amount of monomeric iron species present in solution, because polymeric forms of iron are EPR silent. Furthermore, a change in the features of the EPR spectrum indicates a change in the coordination environment of the iron. Therefore, EPR spectra were used to gain information on the iron-pyrophosphate complex in solution.

Under the experimental conditions used for measurements of the addition of iron-pyrophosphate to apotransferrin, we found that the EPR double integral of the reaction mixture increased over the time course of the reaction. A donor solution of 0.3 mM iron(III) with a PP_i:Fe ratio of 3.7 to 1 at pH 7.4 had an EPR double integral only 41% of that of the 50% iron saturated transferrin product. The same PP_i:Fe solution had a double integral 46% of that of an Fe(EDTA) solution, where all the iron is presumably in the monomeric form. Thus, provided that the double integral accounts for all of the EPR active iron, it appears that less than half of the iron pyrophosphate is in an EPR observable monomeric form under the above conditions of the iron delivery reaction.

At constant pH and iron:pyrophosphate ratio, dilution of a solution of iron pyrophosphate appears to change both the predominant species in solution and the proportion of iron in monomeric form. Figure 1 shows the EPR spectrum of

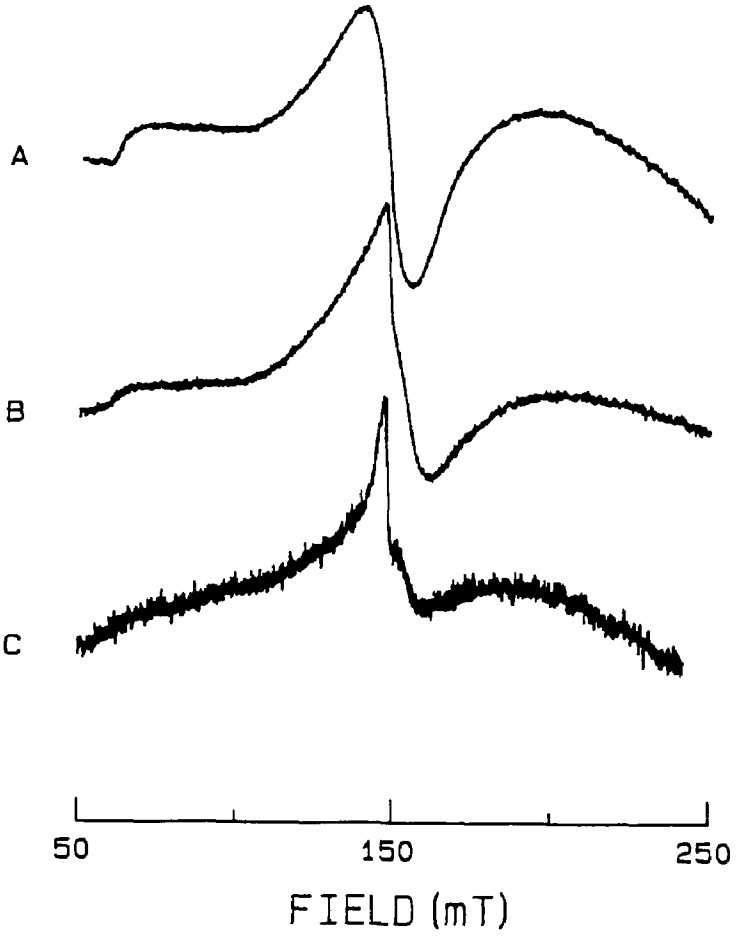

Figure 1.1. The EPR spectrum of iron-pyrophospate solution as a function of dilution. The iron concentration for the solutions corresponding to spectra A, B and C are 8 mM, 1.6 mM and 0.16 mM, respectively. Other solution conditions: Fe:PPi ratio = 1:3.7, pH 7.4, 100 mM Hepes, 20 mM sodium bicarbonate. Instrument settings: power = 20 mW, scan time = 16 min/200 mT, field set = 150 mT, time constant = 1.0 s, modulation amplitude = 1 mT, modulation frequency = 100 kHz, microwave frequency = 9.15 GHz, temperature = 77K, receiver gain = 2000 for A and C and 1000 for B. File C8MM (A), 1P6MM (B), and P16MM (C), disc # 8.

an iron-pyrophosphate solution at pH 7.4 and a PP_i:iron ratio of 3.7:1. The spectra indicate that the iron-PP_i species in solution changes as the solution becomes more dilute. Table I shows values of the double integral as a function of dilution for solutions of iron(III) and pyrophosphate. The proportion of iron in the solution that is EPR active increases as the solution is diluted, indicating increased amounts of monomeric species.

A 3:1 complex of pyrophosphate to iron having the formula $Fe(P_2O_7)_2(HP_2O_7)^{8-}$ (40) is formed in aqueous solution at pH 7.4. An increase in the pyrophosphate:iron ratio is expected to increase the proportion of iron in the monomeric form. However, this does not appear to be the case. Figure 2 shows spectra in which the concentration of iron(III) in both solutions is the same, but the proportion of pyrophosphate is increased from a PP_i ratio of 3.7:1 to 10:1. The double integral for these solutions is essentially the same (Fig. 2 caption), and the spectral characteristics are identical.

Finally, we studied the EPR spectra as a function of temperature at which solutions are prepared. Figure 3 shows EPR spectra of iron pyrophosphate solutions prepared at $0^{\circ}C$ and $25^{\circ}C$. Temperature does not have a significant effect on the iron-pyrophosphate species in solution over this temperature range, the double integrals and spectral shape being similar at both temperatures.

TABLE 1-I

Double Integral for an Iron Pyrophosphate Solution as a Function of Dilution for 3.7:1 Fe:PPi Ratio and pH 7.4

Iron Concentration (mM)	Double Integral ($\times 10^{-7}$)	% Total Iron[#]
0.80	4.15	33
0.42	2.50	38
0.30	2.42	51
0.16	1.69	67
0.032	-	67[@]

[#]Relative to the iron-EDTA double integral, and based on the assumption that 100% of the iron is accounted for in this complex.

[@]Estimated based on the relative peak-to-peak height compared to previous samples. The signal-to-noise was too low in this case to obtain an accurate double integral. For the other samples, the peak-to-peak heights were approximately proportional to the double integral.

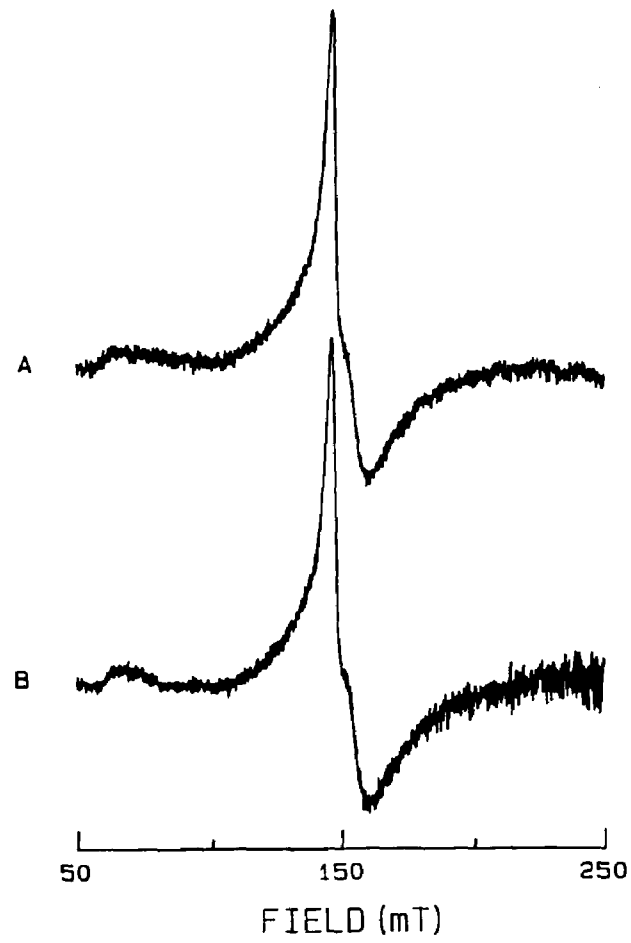

Figure 1.2. EPR spectra as a function of pyrophosphate to iron ratio. Spectrum A has a PPi:Fe ratio of 3.7:1, while spectrum B has a ratio of 10:1; [Fe] = 0.31 mM for both solutions. For other solution conditions and instrument parameters, see Fig. 1. Receiver gain 3200 for A and 5000 for B, temperature = 108K, microwave frequency = 9.101 GHz. Spectra scaled to the same double integral. Double integral, corrected for receiver gain, is 6.3×10^7 for A and 5.7×10^7 for B. File SUE40 (A) and SUE41 (B), disc #8.

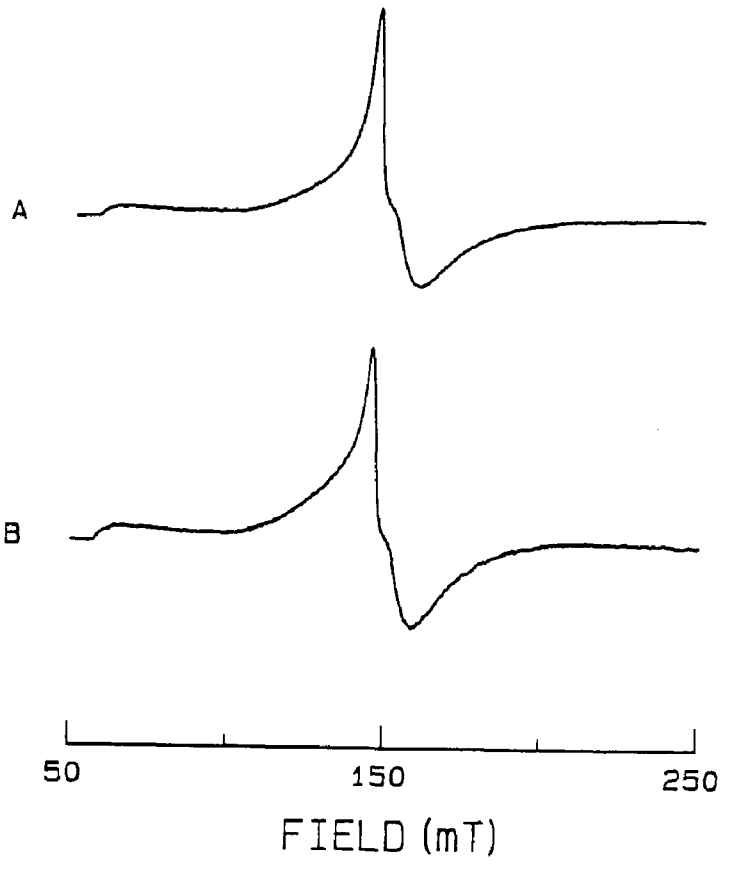

Figure 1.3. EPR spectra of iron pyrophosphate solutions prepared at $0^{\circ}C$ (A) and $25^{\circ}C$ (B). Solution conditions are 0.32 mM Fe(III), 1.2 mM pyrophosphate, 100 mM Hepes, 20 mM bicarbonate, pH 7.4. Instrument settings are the same as in Fig. 1, except receiver gain = 2000. The double integrals are 2.46×10^{7} for (A) and 2.42×10^{7} for (B). File C2.BC (A) and RT1.BC (B), Disc # 8.

Urea-polyacrylamide Gel Electrophoresis

In order to investigate the possibility that the deviation from simple first order kinetics in the second phase of the iron donation reaction was a result of differences between the two iron binding sites, the iron distribution between sites throughout the time course of the reaction was studied by urea-polyacrylamide gel electrophoresis. The results of this experiment are shown in Table II. The iron is directed to the COOH-terminal site relative to the NH_2-terminal site in an average ratio R of 9.5/1. Thus, pyrophosphate is highly site specific in delivering iron to transferrrin, and the EPR spectrum is essentially that of the COOH-terminal monoferric protein.

Reaction Spectra

The reaction of Fe^{3+}-pyrophosphate with apotransferrin-CO_3^{2-} was monitored as a function of time simultaneously by EPR and absorption spectroscopy at 465 nm . Figure 4 shows the family of EPR spectra obtained at $0^{o}C$ in which the protein is brought to 50% saturation; Figure 5 shows the increase in absorbance at 465 nm, as well as a plot of the increase in double integral of the EPR spectrum during the course of the reaction.

The first spectrum of Fig. 4 is that of the reactant $Fe^{3+}(pyrophosphate)_3$. The spectrum of the reaction mixture progressively changes shape and increases in amplitude and integrated intensity (Fig. 5) as the reaction proceeds.

TABLE 1-II

ELECTROPHORESIS DATA: IRON DISTRIBUTION IN A 50% IRON SATURATED SOLUTION OF IRON TRANSFERRIN AS A FUNCTION OF TIME

time	%A*	%C	%N	%D	R+
30 s	55	39	-	10	8.7
50 s	37	51	1	12	9.5
75 s	47	44	1	9	10.7
90 s	36	49	3	13	8.7
105 s	35	49	1	16	7.3
150 s	40	45	3	12	8.5
180 s	27	60	-	12	8.9
4 min	37	51	1	12	9.5
5 min	35	55	-	10	12.2
7 min	32	55	1	13	9.6
20 min	27	57	3	13	9.6
60 min	20	60	2	17	8.0
3 hr (approx)	11	60	4	25	5.8

*A, C, N, and D represent apotransferrin, C-terminal monoferric, N-terminal monoferric, and diferric transferrin, respectively.

+R = Ratio of C-site occupancy to N-site occupancy
= {%C + 0.5(%D)}/{%N + 0.5(%D)}.

Page 63-65, Book II.

After approximately 5 min, the EPR spectrum has a shape similar to that of the product Fe^{3+}-transferrin-CO_3^{2-}, but it continues to grow in intensity. During this phase, the reaction mixture consists primarily of the EPR-active product Fe^{3+}-transferrin-CO_3^{2-} and EPR-silent polymeric iron pyrophosphate (see below).

The presence of an intermediate in the course of the reaction can be illustrated by EPR difference spectroscopy. The difference spectra obtained by subtracting the spectrum of the product from the intervening spectra should have a constant shape but changing amplitude if only two EPR active species are present in solution (see reference 37). A deviation from this behavior is expected when three (or more) EPR active species are present, i.e. monomeric Fe^{3}-(pyrophosphate)$_3$, an intermediate(s), and the product Fe^{3+}-transferrin-CO_3^{2-}.

Figure 6 shows the series of difference spectra for the beginning phase of the reaction in which the spectrum of Fe^{3+}-(pyrophosphate)$_3$ has been subtracted from the others. The sharp features and greater amplitude of the Fe^{3+}-transferrin-CO_3^{2-} spectrum relative to Fe^{3+}-pyrophosphate)$_3$ (cf. top and bottom spectra of Fig. 4) cause the difference spectra (Fig. 6) to have the general features of the spectrum of the product (Fig. 4). However, the lineshape of the difference spectrum progressively changes, becoming much better resolved as the reaction proceeds. This increase in resolution suggests the presence of an underlying signal

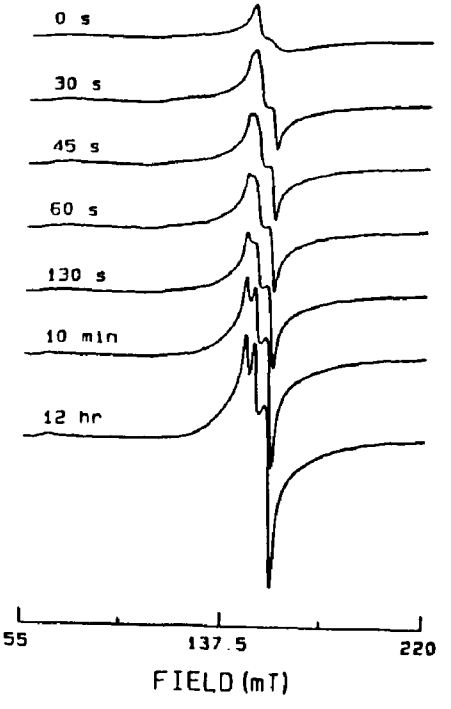

Figure 1.4 EPR spectra as a function of time following mixing of Fe^{3+}-pyrophosphate with apotransferrin. Solution conditions: 0.217 mM apotransferrin, 0.217 mM Fe^{3+}, 0.803 mM pyrophosphate in 0.1 M Hepes, 20 mM $NaHCO_3$, pH 7.40, 0°C. Instrument settings: field set = 150 mT; scan rate = 200 mT/16 min; time constant = 1 s; modulation amplitude = 1.0 mT at 100 kHz; microwave power = 20 mW; and frequency = 9.14 GHz. Files FIVE, SEVEN, EIGHT, TWELVE, NINE and SIX, Disc #1.

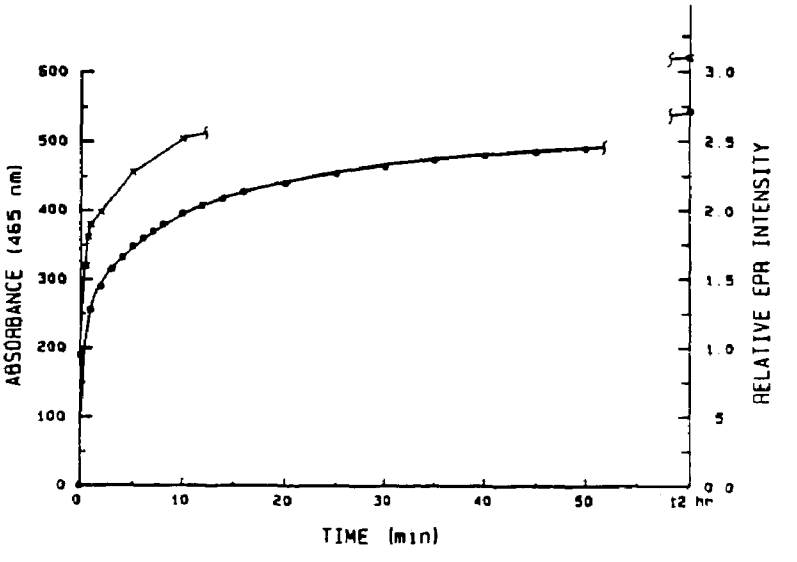

Figure 1.5 Absorbance (●) and EPR intensity(x) as a function of time. Solid line for the absorbance data was calculated from a least-squares fit to equations 1 - 5 using the parameters $k_{2,m}$ = 275 +/- 25 $M^{-1}s^{-1}$, k_1 = 0.014 +/- 0.006 s^{-1}, ϵ_I = 2550 +/- 400 $M^{-1}cm^{-1}$ and the fixed values [T] = 0.217 mM, $[Fe_m]_o$ = 0.096 +/- 0.002 mM, $[Fe_p]_o$ = 0.121 +/- 0.002 mM, $k_{2,p}$ = 14 +/- 0.5 $M^{-1}s^{-1}$. The molar absorptivities of Fe_p and Fe_m = 0; ϵ_P = 2500 $M^{-1}cm^{-1}$. $k_{2,p}$, $[Fe_m]$ and $[Fe_p]$ were determined from Fig. 7. Relative EPR intensity calculated from double integration of the spectra. Conditions as described in the legend to Fig. 4.

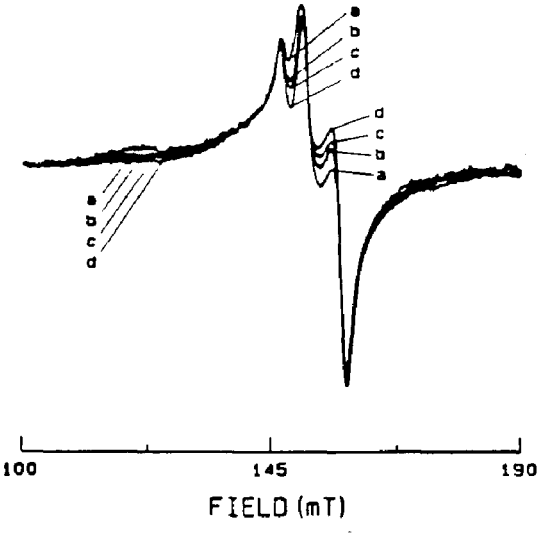

Figure 1.6 EPR difference spectra calculated by subtracting the EPR spectrum of $Fe(PP_i)_3$ from the experimental spectra (Fig. 4) during the beginning phase of the reaction. Spectra scaled to the same peak-to-peak amplitude for ease of comparison of lineshapes. The variation in lineshape indicates the presence of three or more EPR active species, i.e. an underlying signal from an intermediate(s). (a), 30 s; (b), 45 s; (c), 60 s; and d, 130 s. File SEVEN, EIGHTR, NINE and TEN.SUB, disc #1.

which decays in time. We ascribe this signal to the presence of a transient intermediate. After 5 min the signal attributed to the intermediate(s) has mostly decayed away; the difference spectrum changes no further and is similar in shape and resolution to that of the product Fe^{3+}-transferrin-CO_3^{2-}.

Kinetic Analysis

Since both monomeric and polymeric iron(III) pyrophosphate complexes are present, the delivery of iron to transferrin is expected to follow two pathways. Assuming second order formation of intermediate and first order decay to product, the following reaction sheme is proposed:

Rapid pathway:

$$\underset{[Fe_m]}{Fe(PPi)_3}\ (\text{monomer}) + \underset{[T]}{TRF\text{-}CO_3^{2-}} \xrightarrow{k_{2,m}}$$

$$\underset{[I]}{PP_i\text{-}Fe^{3+}\text{-}TRF\text{-}CO_3^{2-}} \xrightarrow{k_1} \underset{[P]}{Fe^{3+}\text{-}TRF\text{-}CO_3^{2-}}$$

Slow pathway:

$$\underset{[Fe_p]}{Fe\text{-}PP_i}\ (\text{polymer}) + \underset{[T]}{TRF\text{-}CO_3^{2-}} \xrightarrow{k_{2,p}}$$

$$\underset{[I]}{PP_i\text{-}Fe^{3+}\text{-}TRF\text{-}CO_3^{2-}} \xrightarrow{k_1} \underset{[P]}{Fe^{3+}\text{-}TRF\text{-}CO_3^{2-}}$$

Here $[Fe_m]$ and $[Fe_p]$ are the concentrations of monomeric and polymeric Fe^{3+} pyrophosphate, which react with the transferrin-carbonate complex T according to the second-

order processes having rate constants $k_{2,m}$ and $k_{2,p}$, respectively, where $k_{2,m} \gg k_{2,p}$. An intermediate I formed in both pathways decays to product P by a first-order process with a rate constant k_1. The buildup of intermediate is insignificant by the slow pathway because its formation is slow relative to its decay. The coupled differential equations which describe the kinetics are given by

$$-d[T]/dt = k_{2,m}[T][Fe_m] + k_{2,p}[T][Fe_p] \quad [1]$$

$$d[I]/dt = k_{2,m}[T][Fe_m] + k_{2,p}[T][Fe_p] - k_1[I] \quad [2]$$

$$d[P]/dt = k_1[I] \quad [3]$$

$$-d[Fe_p]/dt = k_{2,p}[T][Fe_p] \quad [4]$$

$$-d[Fe_m]/dt = k_{2,m}[T][Fe_m] \quad [5]$$

These equations cannot be solved in closed form. Accordingly, they were integrated numerically in increments of 0.1 s with a computer program to give the concentrations of all species as a function of time for a given set of rate constants and initial concentrations. The input parameters $k_{2,m}$, k_1*, and ϵ_I, where ϵ_I is the molar absorptivity of the intermediate, were varied iteratively to give a least-squares fit to the 0°C absorbance data (Fig. 5). The other parameters in the model were determined independently (see

*k_1 was estimated from the difference spectra (Fig. 6). Since $\epsilon_I \sim \epsilon_P$, the absorbance is insensitive to this process.

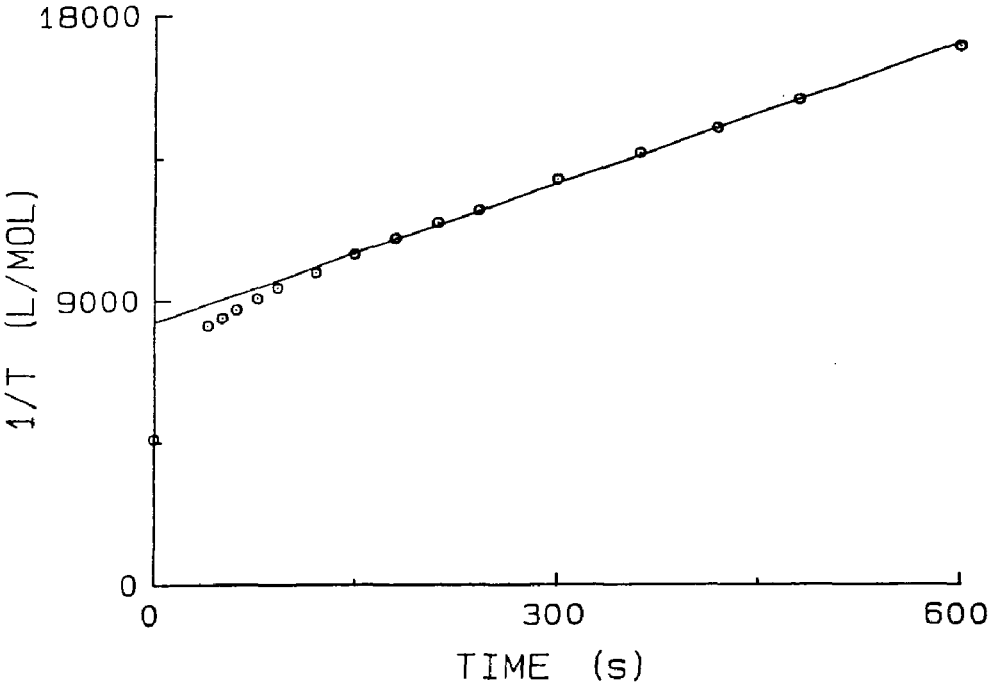

Figure 1.7 1/[T] <u>versus</u> time plot for the second-order reaction of the absorbance data at 465 nm from Fig. 5. Least squares fit using points beyond 90 s, gives a slope = 14.7 +/- 0.5 $M^{-1}s^{-1}$ and a y-intercept = 8300 +/- 160 M^{-1}; correlation coefficient = 0.999. Uncertainties are the 95% confidence interval. The intercept corresponds to $[Fe_m]_o$ = 0.096 +/- 0.002 mM, and $[Fe_p]_o$ = 0.121 +/- 0.002 mM. File 2ND, disc 385.

below) and held fixed.

The rate constant k_{2p} was obtained from a linear least-squares fit of 1/[T] *versus* time plot for the second-order reaction of the second phase (Fig. 7 & 8). Since formation of intermediate by the rapid pathway is essentially complete within the first minute and less than 5 % of the product has been formed by the slow pathway in this time interval, it is reasonable to consider the slow pathway to be independent of the fast reaction. Therefore, an estimate of the initial concentration of polymeric iron was made by extrapolation of 1/T *versus* time plot (Fig. 7 & 8); $[Fe_p]_o$ is the inverse of y-intercept, and $[Fe_m]_o$ is the difference between $[Fe_p]_o$ and the total iron concentration.

The model reproduces the data very well (Fig. 5). The rapid pathway gives rise principally to the first phase and the slow pathway to the second phase. The molar extinction coefficient of the intermediate at 465 nm is comparable to that of the product.

The EPR spectra of Fig. 4 were deconvoluted to obtain the spectrum of the intermediate. By using molar fractions calculated from the curve-fitting parameters (Figs. 5 and 7) as a guide, spectra of the EPR active reactant Fe_m and product P were appropriately weighted and subtracted from the spectrum of the reaction mixture. The spectrum of the intermediate obtained in this way for various times is shown in Fig. 9. The spectra all have the same principal features, giving us confidence that the analysis is correct. Moreover, the spectrum of the putative intermediate is

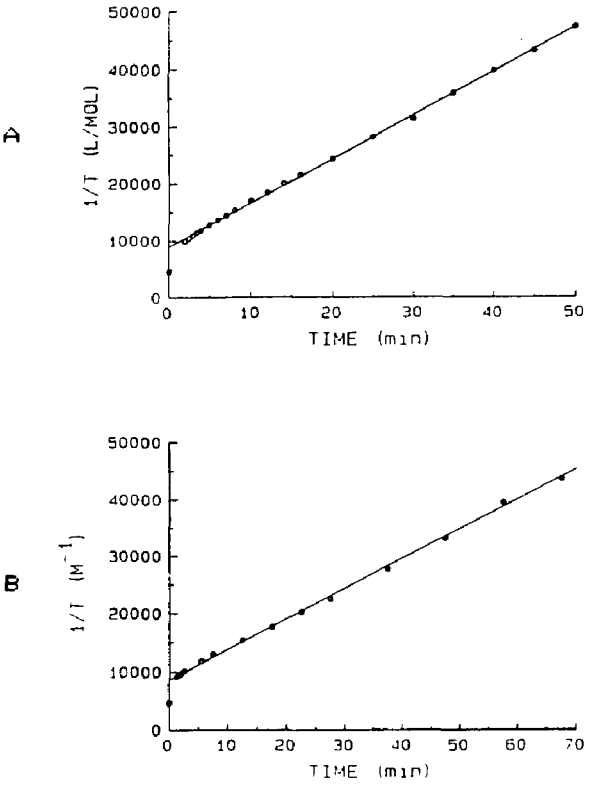

Figure 1.8 1/[T] versus time for absorbance data at 465 nm (A) and 245 nm (B). Solution conditions are as described in Fig. 5. A is the same as in Figure 7, except the data is over a longer time period. For the 245 nm data (B), the slope is 8.7 +/- 0.2 $M^{-1}s^{-1}$, the y-intercept is 8700 +/- 300 M, correlation coefficient, using values beyond 1 min, is 0.999. Files 46520 and 24520, disc 6-86.

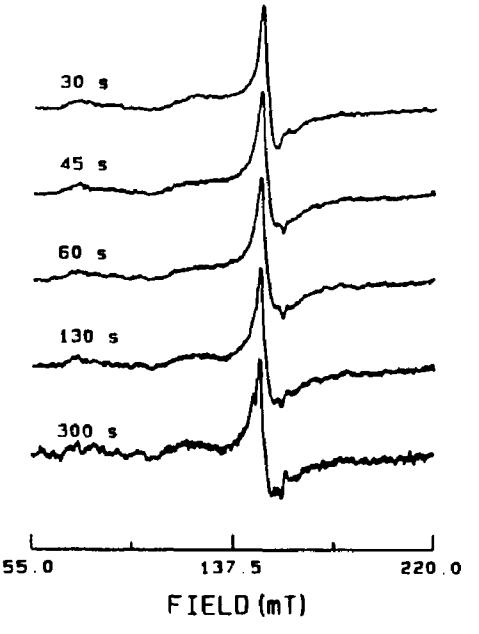

Figure 1.9 Spectrum of the putative intermediate calculated by deconvoluting the experimental spectra at various times. The same spectrum is obtained in all cases. The percent of EPR-active species which is the intermediate varies from 28% at 30 s to 4% at 300 s. The intermediate is continually forming and subsequently decaying to product in this time interval. Spectra scaled to the same peak-to-peak amplitude. File SEVEN, EIGHT, NINE, TEN, AND ELEVEN.PUB, disc # 1.

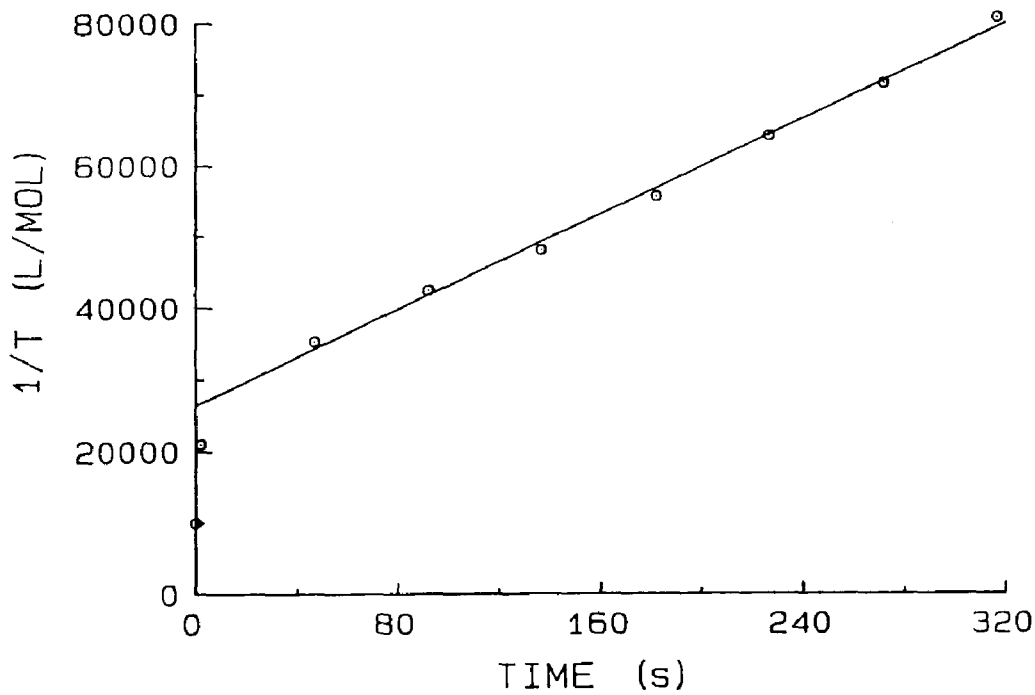

Figure 1.10 1/T <u>versus</u> time plot for the second order reaction at 25°C. Slope = 167 +/- 12 $M^{-1}s^{-1}$, y-intercept = 26400 +/- 2400 M; correlation coefficient = 0.998. Conditions: $[Fe^{3+}]$ = 0.1 mM, $[PP_i]$ = 0.4 mM, [apotransferrin] = 0.1 equivalents/liter, 20 mM sodium bicarbonate, 20 mM Hepes, pH 7.4. Raw data are from absorbance readings taken at 460 nm. From reference 37, Fig. 2. File GB2ND, disc 6-86.

different from that of either the reactant or product (cf. Figs. 4 and 9). The half-life of the intermediate as estimated from the EPR data is approximately 1.5 min at 0°C.

A second-order plot of the addition of iron-pyrophosphate to apotransferrin at 25°C is shown in Fig. 10. The second-order rate constant has increased about ten-fold for a 25° rise in temperature, which corresponds to an activation energy of approximately 66 kJ-mol^{-1}. The initial concentration of polymeric iron estimated from the y-intercept is 38% for a solution of 0.1 mM iron with an iron:PP_i ratio of 1:4. This result compares with approximately 33 % in polymeric iron at iron concentrations in the range between 0.032 mM and 0.16 mM (Table I). Thus the kinetic data are consistent with the finding that the monomeric form of iron pyrophosphate increases as a result of dilution, with no apparent change as a function of temperature between 0°C and 25°C.

The nature of the putative intermediate

Because the g' = 4.3 signal of high spin iron compounds is not well understood, it is not possible to draw conclusions about iron coordination in the intermediate from the EPR spectrum alone. However, the following data may shed some light on the nature of the intermediate. Figure 11 shows the EPR spectrum of iron-pyrophosphate in the presence of 25% glycerol; the spectral characteristics of this complex are similar to those of the intermediate. The

presence of glycerol is known to increase the viscosity of a water solution and occasionally alter the EPR spectrum, presumably by affecting the freezing process and solute aggregation. Since the presence of the protein also increases the viscosity of a water solution, we needed to see whether our "intermediate" was merely a perturbation of the EPR spectrum due to the increased viscosity of the solution. Two experiments were designed and carried out to address this question.

First, a stopped flow apparatus was used to measure the EPR spectrum of the iron pyrophosphate complex in the presence of apotransferrin in the very initial stages of the reaction, before any appreciable formation of product had occurred (See Materials and Methods). The residence time of the reactants in the mixing chamber was approximately 1 s. The EPR spectrum of the crystals rapidly frozen in a pentane slush was measured (Fig. 12). There is no evidence of an intermediate-like spectrum (cf. Figs. 9 and 12).

In a second experiment, the EPR spectrum of iron-pyrophasphate was measured in the presence of 30 mg/ml of bovine serum albumin (BSA). BSA is expected to increase the viscosity of a water solution; but, unlike transferrin, BSA does not have a specific iron-binding site. It is therefore expected that the iron-pyrophosphate spectrum would reflect perturbations similar to those seen for transferrin in the absence of the iron-binding at the specific site. These results are shown in Fig. 13. Again, we see no evidence of an intermediate-like signal.

From the data presented above, it appears unlikely that the intermediate signal is a result of general changes in the solution conditions resulting from the presence of the protein. The changes in the EPR spectrum of iron-pyrophosphate in the presence of glycerol probably involve specific interactions between glycerol and the iron-pyrophosphate complex. Glycerol is known to be a ligand for iron(III), and the high concentration of glycerol relative to pyrophosphate may allow the glycerol to compete effectively for coordination positions on the metal.

Furthermore, the similarity of the putative intermediate EPR spectrum to that of iron-pyrophosphate in glycerol does not necessarily indicate that the metal coordination is the same in these compounds. Unlike other forms of spectroscopy (e.g. IR or NMR), EPR spectra are not uniquely indicative of particular chemical forms. It is sometimes the case that compounds very dissimilar in metal coordination will have similar EPR spectra (43).

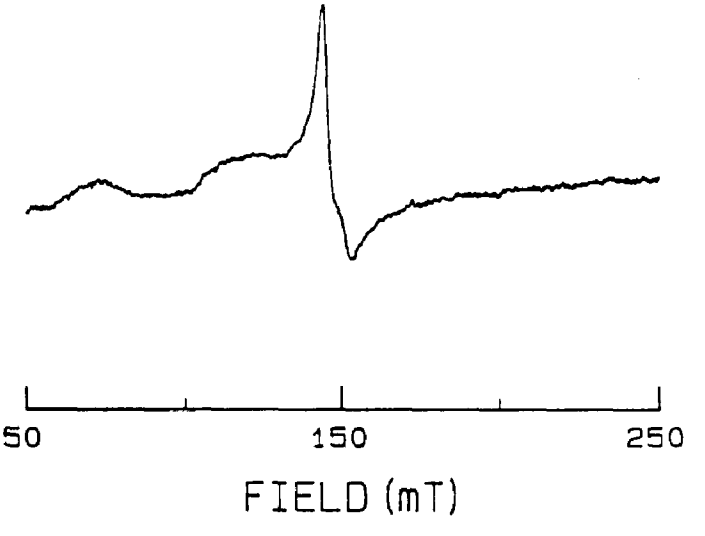

Figure 1.11 EPR spectrum of a solution of iron-pyrophosphate in 25% glycerol. Solution conditions: 0.6 mM Fe^{3+}, 2.3 mM pyrophosphate, 75 mM Hepes, 15 mM sodium bicarbonate, pH 7.4. Spectrometer settings same as in Fig. 1, except receiver gain = 1000, scan range = 400 mT, field set = 200 mT, and scan time = 16 min/400 mT. Only the central portion of the spectrum is shown above. File T04000, disc # 8.

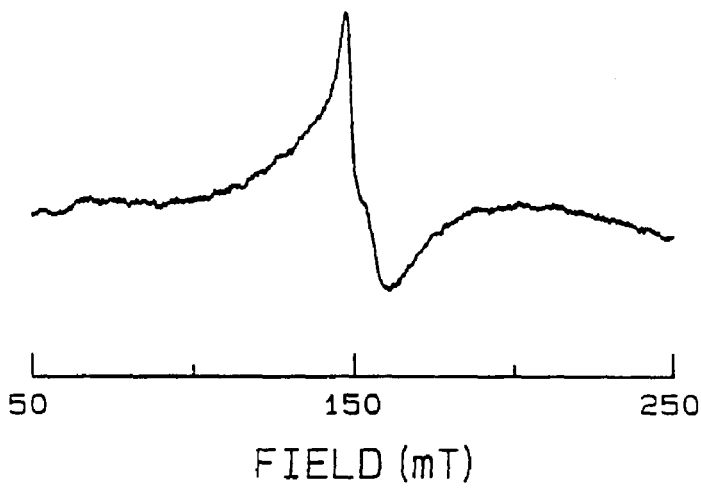

Figure 1.12. EPR spectrum obtained in a stopped flow apparatus immediately after mixing of iron-pyrophosphate and apotransferrin. For further details, see text. Solution conditions: [apotransferrin] = [Fe^{3+}] = 0.68 mM, [pyrophosphate] = 2.52 mM, in 100 mM Hepes, 20 mM sodium bicarbonate, pH 7.4. Spectrometer settings the same as in Fig. 1, receiver gain 4000. File PPI111.BC., disc 6-84.

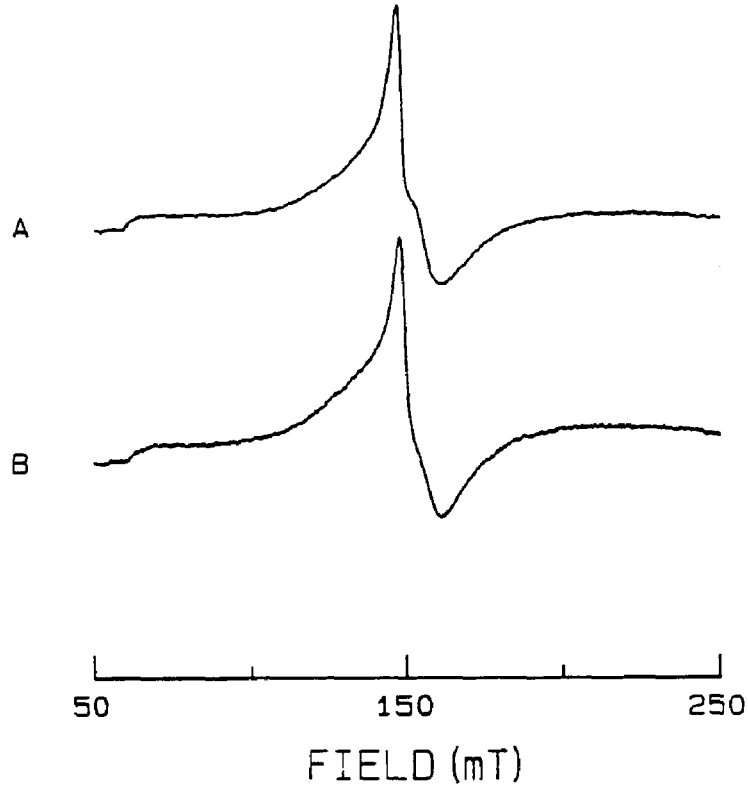

Figure 1.13. EPR spectrum in the absence (A) and presence (B) of 30 mg/ml of BSA. Solution conditions: 0.32 mM Fe^{3+}, 1.18 mM pyrophosphate, 100 mM Hepes, 20 mM sodium bicarbonate, pH 7.4. Instrument settings same as in Fig. 1, receiver gain = 4000. File 12SS and 13SS, disc # 5.

DISCUSSION

The formation of mixed ligand complexes is probably a common feature of metal ion exchange reactions between chelators and transferrin. We do not know whether iron is bound to both pyrophosphate and the protein in the intermediate. The EPR spectrum of the intermediate (Fig. 9) lacks the three-component feature of the fully developed Fe^{3+}-transferrin-CO_3^{2-} complex, indicating a difference in coordination environment of the Fe^{3+}. The Fe^{3+}-transferrin-anion complexes in which carbonate has been replaced by other anions are known to exhibit markedly different EPR spectra (31). Thus it appears that ligand substitution in only one coordination position can substantially alter the EPR spectrum. Loss of structure in the EPR signal of the C-terminal site has also been observed upon binding of lyotropic anions such as perchlorate to sites on the protein (28,41,42). Based on the EPR spectrum alone, it is therefore not possible to conclude how pyrophosphate is bound in the intermediate complex. Both allosteric sites and direct coordination to the iron may be involved.

The similarity of the EPR spectrum of the intermediate to that of iron-pyrophosphate in glycerol suggests that pyrophosphate may still be bound to the iron in the intermediate. It is possible that the oxygen donor atoms of glycerol coordinate to the iron in a manner similar to tyrosine ligands on the protein. Our simulation suggests

that two tyrosines are complexed to the iron in the intermediate, since the molar absorptivity at 465 nm is estimated to be the same as that for Fe^{3+}-transferrin-CO_3^{2-} in which two tyrosines are coordinated (27). The BSA and stopped flow data suggest that the intermediate is not a result of non specific binding to the protein. Therefore, it appears probable that the intermediate involves interaction with ligands in the region of the specific iron binding site and that pyrophosphate remains attached to the iron in this complex.

A reaction mechanism consistent with our data can be postulated: The highly negative $Fe(PP_i)_3^{8-}$ complex is directed toward the cluster of cationic groups located near the iron binding region (13). The tyrosine groups which are ligands to the iron in the fully coordinated metal are particularly good ligands for iron(III) and readily displace the pyrophosphate ligand(s). Positively charged amino acids in the region probably faciliate the iron transfer by stabilizing the pyrophosphate ligand during the iron exchange reaction. The intermediate seen in the EPR is this PP_i-Fe-transferrin species in an "open" conformation, where at least one coordination position is different from that of the fully cordinated iron in the stable complex. The protein must then fold into the "closed" form, in which the final histidine(s) is bound to the iron and pyrophosphate is released (14); this process follows a first order decay.

It is known from chemical modification studies that

negatively charged anions such as perchlorate are directed toward the tyrosines in the iron binding region (44). Hydrodynamic data (45) and kinetic evidence (46), as well as a string model of transferrin based on the amino acid sequence (13), indicate that transferrin exists in an "open" conformation prior to metal coordination, and that the molecule assumes a more compact conformation upon iron binding. Furthermore, if the above mechanism is correct, it is clear why pyrophosphate is such a good mediator for iron exchange with transferrin. Pyrophosphate is both a good ligand for iron and has high affinity for the anion binding site. Also, the complex formed with pyrophosphate has a high negative charge, which likely plays an important role in the mechanism of iron exchange.

CHAPTER II

EPR STUDY OF THE LOW SPIN ADDUCT FORMED BY ADDITION OF CYANIDE TO DIFERRIC TRANSFERRIN

INTRODUCTION

Iron(III) specifically bound to transferrin was first shown to be high spin by Ehrenberg and Laurell in 1955 using room temperature magnetic susceptibility measurements (47). Subsequently, EPR (26,48) and Mossbauer (49,50) measurements have confirmed this finding. More recently, Harris, in a preliminary study, demonstrated that cyanide forms an adduct with diferric transferrin which was shown by EPR to be low spin (4). He postulated that cyanide may replace water in the first coordination sphere of the metal.

The ground state of iron(III) complexes can exhibit either high spin or low spin behavior, depending on the strength of the ligand field. As the ligand field strength increases, low spin complexes are increasingly favored. Generally, ligands such as CN^- or CO, which are strong sigma donors and strong pi acceptors, produce the strongest ligand fields (51). Low spin complexes of iron(III) are rather unstable and are easily reduced to iron(II). While iron(III) usually exhibits high spin behavior, low spin iron(III) complexes can be prepared using strong field ligands. Thus, $Fe(CN)_6^{3-}$, $Fe(phen)_3^{3+}$, $Fe(bipy)_3^{3+}$ and $Fe(en)_3^{3+}$ are low spin complexes (52,53), while Fe(EDTA) and weaker field ligand complexes usually are high spin.

The iron porphyrin protein cytochrome 450 has been shown by EPR to undergo change from a low-spin to a high-spin state as a result of substrate binding (54). The low spin ferric heme complex has an EPR signal typical of low

spin ferric complexes where sulfur is one of the axial ligands (g_1 = 2.45, g_2 = 2.26, and g_3 = 1.91). Upon binding of the substrate camphor, it is likely that a conformational change in the protein results in removal of a cysteine ligand and the resultant change to low spin behaviour (55). The g-values for the low spin complex are insensitive to changes in the non-mercaptide ligand in the axial position and indicate a high degree of rhombic distortion (54).

Schiff bases form complexes with most transition metals (56) which, like transferrin, involve metal coordination with both oxygen and nitrogen ligands. However, most of these Fe(III) complexes are low spin because of the strong ligand field produced by the doubly bonded nitrogen. They also exhibit deviations from axial symmetry (57). Nishida et al. have prepared low-spin iron(III) complexes using quadridentate Schiff bases (see Figure 1 and Table I) (58). In these complexes, the metal coordinates to oxygen and nitrogen in the equatorial positions.

EPR studies of these compounds show that all are low spin and have rhombic g-tensors. Furthermore, the g-values are quite insensitive to changes in the ligands. For all compounds studied, the g values fall within the range: g_1 = 2.3~2.4, g_2 = 2.1~2.2, and g_3 = 1.9~2.0 (See Table II). By using Kotani's method for correlating the g values with occupation of the molecular orbitals (59), Nishida et al. found that the unpaired electron resides mainly in the d_{xy} orbital, independent of the axial ligand. Occupation of the

d_{xy} orbital places electron density between the metal ligand axes in the equatorial plane of the molecule.

Similarly, studies of substituted Fe(III) porphyrins showed that the unpaired electron for these complexes is largely d_{yz} orbital based (60,61), also independent of axial ligands (62). From these two cases, it thus appears that the equatorial ligands dominate the energy of the t_{2g} orbitals in iron(III) complexes of these types.

Nishida et al. have also synthesized several iron(III) Schiff base complexes which exhibit spin crossover (63). In these complexes, there is an equilibrium between the high spin and low spin states which is temperature dependent. In terms of the ligand field strength, these compounds are very near the border between high spin and low spin states, and thus both states are thermally accessible. The most dramatic change occurred for $[Febzacen(im)_2]BPh_4$, where the u_{eff} increased from ~2 at 77K to ~4.5 at 295K. A u_{eff} of approximately 2.3 B.m. corresponds to S = 1/2, whereas for S = 5/2, the u_{eff} is approximately 5.9 B.m. Similar spin equilibria occur in iron porphyrin compounds (64).

The purpose of this study was to characterize further the low spin adduct formed by addition of cyanide to diferric transferrin in order to gain additional insight into the nature of the metal site. While cyanide may replace water in the specifically bound site of transferrin (4), our work indicates that cyanide is replacing carbonate that is generally thought to be a bridging ligand between

iron and a positively charged amino acid residue on the protein. This is a significant finding for two reasons. First, it suggests that iron bound to the specific site of transferrin is accessible to iron chelators present in the surrounding media. This provides a mechanism by which chelators could play a role in iron release in vivo. Second, provided iron remains at the specific iron binding site in the adduct, this study refutes the generally accepted notion that iron binding cannot occur in the absence of bicarbonate or a "bicarbonate-like" anion.

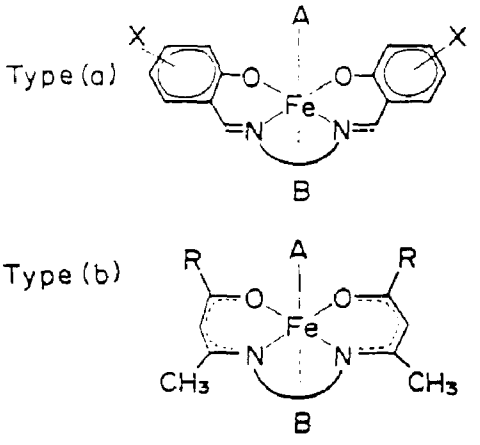

Figure 2.1 Low spin iron (III) complexes formed from quadridentate Schiff bases. See Table I for values of X and R. From reference 58.

Table 2-I

STRUCTURE AND ABBREVIATIONS OF QUADRIDENTATE LIGANDS

Quadridentate Schiff Base - Type A	X
N,N'-bis(salicylidene)ethylenediamine H_2salen	H
N,N'-bis(3-methoxysalicylidene)ethylemediamine H_2vanen	3-CH_3O

Quadridentate Schiff Base - Type B	R
N,N'-bis(1-acetonylethylidene)ethylenediamine H_2acen	CH_3
N,N'-bis(2-benzoyl-1-methylethylidene)ethylenediamine H_2bzacen	C_6H_5

Unidentate Ligands
Imidazole im
4-Aminopyridine apy

Table 2-II

G-values for Iron(III) Schiff Base Complexes
(See Figure 1 and Table I)
(from reference 58)

Complexes	g_1	g_2	g_3
Na[Fesalen$(CN)_2$]	2.25	2.15	1.99
[Fevanen$(im)_2$]BPh_4*	2.44	2.21	1.89
[Feacen$(im)_2$]BPh_4	2.36	2.14	1.94
[Feacen$(apy)_2$]ClO_4	2.31	2.10	1.91
Na[Feacen$(CN)_2$]	2.32	2.13	1.96
[Febzacen$(im)_2$]BPh_4*	2.40	2.10	1.94
[FebzacenCN(im)]	2.35	2.09	1.94

*These measurements were taken at 77K. All others were taken at 295K.

MATERIALS AND METHODS

All chemicals were reagent grade and obtained from the following sources:

sodium bicarbonate - Baker Analyzed Reagents
sodium cyanide - Fisher Certified Reagents
Hepes (N-2-hydroxyethyl piperazine-N'-2-ethane sulfonic acid) - Research Organics
ferrous ammonium sulfate - Baker Analyzed Reagents
iron atomic absorption standard (1000 ppm) - Fisher Certified Reagents
nitrilotriacetic acid (NTA), disodium salt - Sigma Grade
sodium sulfate - Fisher Certified Reagents
sodium thiocyanate - Fisher Certified Reagents

Except for sodium cyanide solutions, reagent solutions were routinely treated with Chelex 100 prior to use. The Chelex was separated from the solutions by allowing it to settle and then carefully pipetting the supernatant. Glassware was soaked in 50% HCl and rinsed thoroughly. Water was doubly deionized (D/D) with a conductance greater than 2×10^6 ohm-cm. Carbon dioxide free water was prepared by boiling D/D water for a minimum of fifteen minutes; the hot water was then cooled under dinitrogen or argon.

Transferrin

Human serum apotransferrin of 98% stated purity was obtained from Calbiochem-Behring and used without further purification. The concentration was determined spectrophotometrically on a Spectronic 200 or Cary 219 spectrophotometer using $\epsilon^{280nm} = 9.07 \times 10^4$ $M^{-1}cm^{-1}$, calculated from the absorbance of a one percent solution, 11.4 (65), and the molecular weight, 79,600 (7).

Diferric transferrin was prepared by slow addition, with stirring, of 1.8 equivalents of 0.02M ferrous ammonium sulfate (in 0.01M HCl) to apotransferrin in 25mM sodium bicarbonate, 20-100 mM Hepes, pH 7.4. After 24 hours, the percent saturation was determined using ^{465}= 5000 $M^{-1}cm^{-1}$ per two iron(III) bound (31). The diferric solution was then ultrafiltered with CO_2 free D/D water using an Amicon ultrafiltration cell with a PM10 membrane until the concentration of Hepes was <0.1% of the original. The pH was adjusted to 10.4 with 1M NaOH with stirring. This stock protein solution was stored in a freezer at -20°C. The stock protein solution was thawed and the pH adjusted under argon or dinitrogen prior to an experiment.

Preparation of Adduct

Since HCN is a volatile and toxic gas, manipulations involving cyanide solutions were carried out in the hood. Sodium cyanide was dissolved in water, and then the pH was brought down slowly to 10.4 using 1M HCl. The diferric transferrin at pH 10.4 was then mixed with the appropriate amount of sodium cyanide and water for dilution. This was typically done in an argon-filled EPR tube. The EPR tube was then capped using a serum stopper and shaken vigorously. Developed samples were frozen in dry ice/acetone and stored at -100°C in a Revco freezer. When not specified, the concentration of carbonate was a constant minimal value.

Bicarbonate Dependence

For the bicarbonate equilibrium studies, the diferric protein was placed to an ultrafiltration cell along with the specified bicarbonate concentration and then the appropriate amount of sodium cyanide solution was added. All solutions were pH adjusted before mixing. Then, the bicarbonate concentration was decreased by ultrafiltration with a "bicarbonate-free" sodium cyanide solution added such that the sodium cyanide concentration in the cell remained constant. The ultrafiltration and all solution transfers were done using purified argon gas (Wesco). Dilution of bicarbonate was calculated by measuring the amount of ultrafiltrate removed and the amount of sodium cyanide solution added for each point. For each point in the titration, an aliquot was removed from the cell, placed in an EPR tube, and frozen in dry-ice/acetone. This aliquot was then returned to the ultrafiltration cell after measurement.

Cyanide Dependence

The cyanide equilibrium studies were carried out in individual EPR tubes. The diferric protein, water for dilution, and sodium cyanide solutions were added to the EPR tubes and shaken vigorously using wrist action. All samples were developed for 90 minutes at room temperature, then frozen in dry ice/acetone.

EPR Measurements

EPR measurements were taken on a Varian E-4 spectrometer interfaced to a MINC-23 computer. A liquid nitrogen Dewar insert was used for measurements at 77K. For the variable temperature work, a Varian liquid nitrogen flow through system was used; the temperature controller was calibrated using a copper-constantan thermocouple. EPR Spectrometer settings were:

Field Set	2500 Gauss
Scan Width	4000 Gauss
Time Constant	1 s
Modulation Amp.	12.5 Gauss
Scan Time	16 min
Power	20 mW

Except for the variable temperature work, all EPR measurements were taken at 77K. 2500 data points were collected over the 4000 Gauss range; all spectra were stored on floppy disc. Double integrals were taken on baseline corrected spectra assuming a liniar deviation in the baseline.

EPR tubes were matched according to inner and outer diameters, and then calibrated to one another using a diferric transferrin solution of approximately 0.5 mM. When signal intensities or double integrals were compared using different tubes, corrections were made using the appropriate calibration factor. Calibration factors ranged

from 0.943 to 1.035. In order to correlate double integrals with actual concentration of native iron transferrin and cyanide adduct, an Fe_2-transferrin standard was used for the g=4 high-spin region and a copper chloride solution (1:2 v/v glycerol/water, pH 2.0) was used for the g=2 low-spin region. For the copper standard, a 1.00 mM sample at a gain of 100 had a double integral of 9.50×10^6 when integrated between array points 1200 and 2000. The diferric transferrin standard, which was 1.00 mM in iron as determined by the absorbance at 465 nm, had a double integral of 5.08×10^6 when integrated between array points 10 and 1200.

RESULTS

Evidence for Formation of a Specific Cyanide Adduct

The initial experiments involved duplication of the work by Harris, with minor modifications. An inverse relationship between the bicarbonate concentration and the ease of adduct formation was observed, i.e. the adduct could be formed at lower cyanide concentration if the bicarbonate concentration was minimized (66). Figure 2 shows an EPR spectrum of a sample which was prepared as described in the Materials and Methods section; approximately half of the iron in the solution is in the high spin form and shows an EPR spectrum in the g = 4.3 region typical of iron transferrin. The other half of the iron resonates in the g = 2 region showing a spectrum typical of a low-spin Fe(III) complex with rhombic symmetry. This data and the corresponding g-values for the low-spin adduct are consistent with the results of Harris(4).

In order to verify that the low spin EPR signal arose from an iron protein complex and not from a low molecular weight chelate, two experiments were performed. In the first experiment, a sample which contained both iron transferrin and the adduct was ultrafiltered using a PM 10 membrane with a nominal molecular weight exclusion limit of 10,000. The volume was reduced by 60%. EPR spectra were taken of the retentate before (Figure 3A) and after (Figure

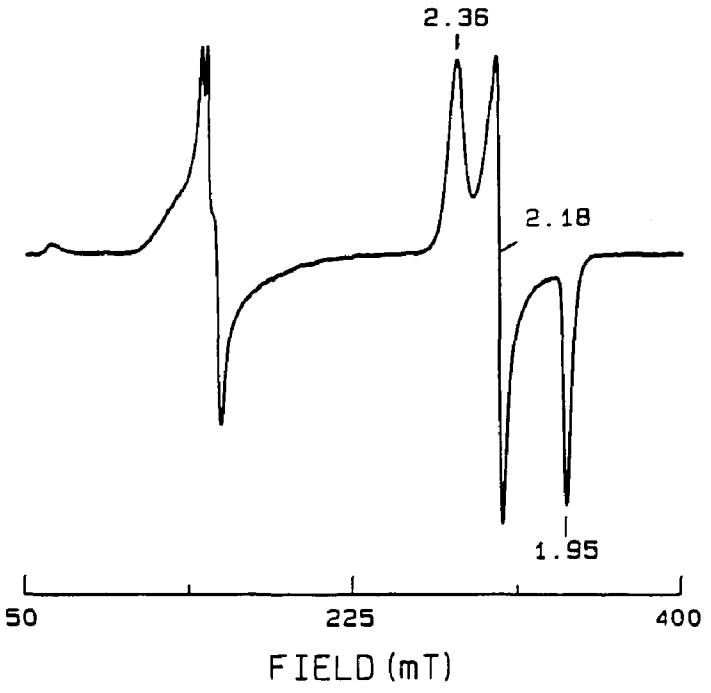

Figure 2.2 EPR spectrum of iron transferrin in the presence of 0.82 M NaCN at pH 10.6. 47% of the iron is low spin as determined by the double integral. The protein concentration is 0.58 mM, 90% iron saturated. Instrument gain is 500. File 7G.BC, disc 12-85.

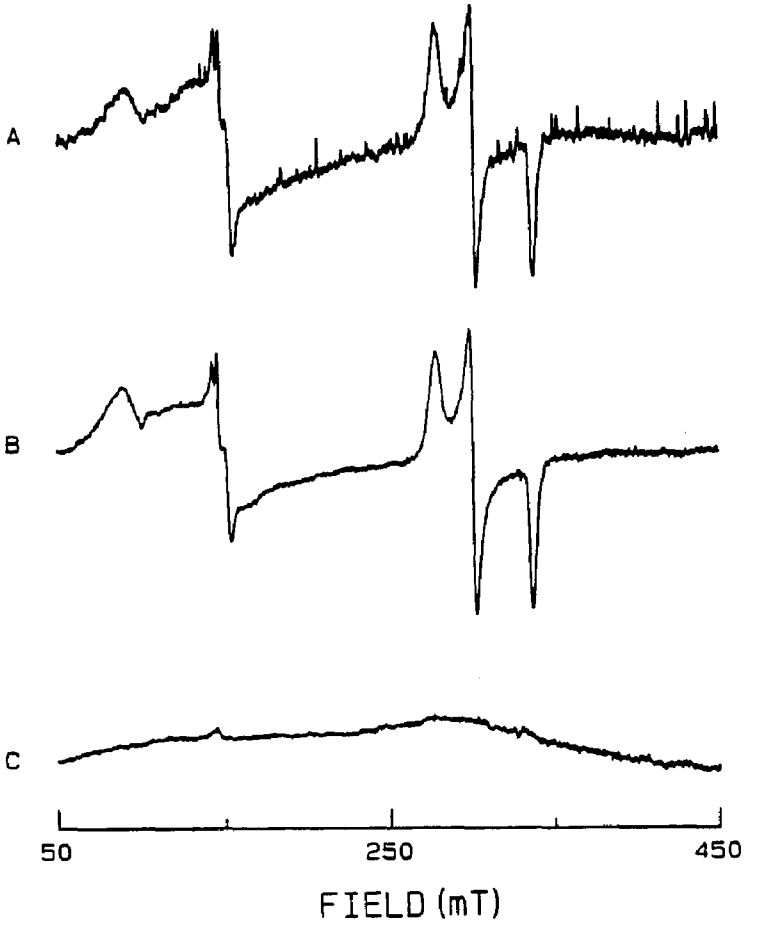

Figure 2.3 Ultrafiltration experiment. Spectrum A is the sample of diferric transferrin in the presence of cyanide before ultrafiltration, B is the retentate after the sample volume had been reduced by 60%, and C is the filtrate. Conditions: 0.4 M NaCN, pH 11, protein concentration is approximately 0.1 mM for A and 0.25 mM for B. Instrument gain = 3200. File PREUF, POSTUF, and THRUUF, disc 3-85.

3B) the ultrafiltration, and of the ultrafiltrate (Figure 3C). The g=2 portion of the spectrum is associated with the protein since no spectrum is observed with the ultrafiltrate.

In the second experiment, ultrafiltration was done with a solution containing iron(III) and cyanide but not protein. It was discovered that a rhombic EPR low spin iron(III) signal very similar to the adduct signal could be generated by simply mixing iron chloride in HCl with 1M sodium cyanide at pH 11. In order to preclude the possibility that the "adduct" was due to such a species, a solution of iron(III) chloride in cyanide was ultrafiltered. Identical EPR spectra were obtained with the retentate and ultrafiltrate indicating that the membrane is permeable to this species.

Evidence for Adduct Formation in One Site

It was not possible to convert diferric transferrin to more than 50% adduct, regardless of the cyanide concentration. The average percent adduct formation was 47% at cyanide concentrations in excess of 0.5M. Therefore, it seems likely that the adduct is formed at only one site. The possibility that adduct formation at either site then prevents adduct formation at the other site cannot be excluded, however.

To gain some insight into which site forms the adduct, an experiment was done in which cyanide was added to a diferric transferrin solution in the presence of thiocyanate. Effects of thiocyanate (Fig. 4B) and

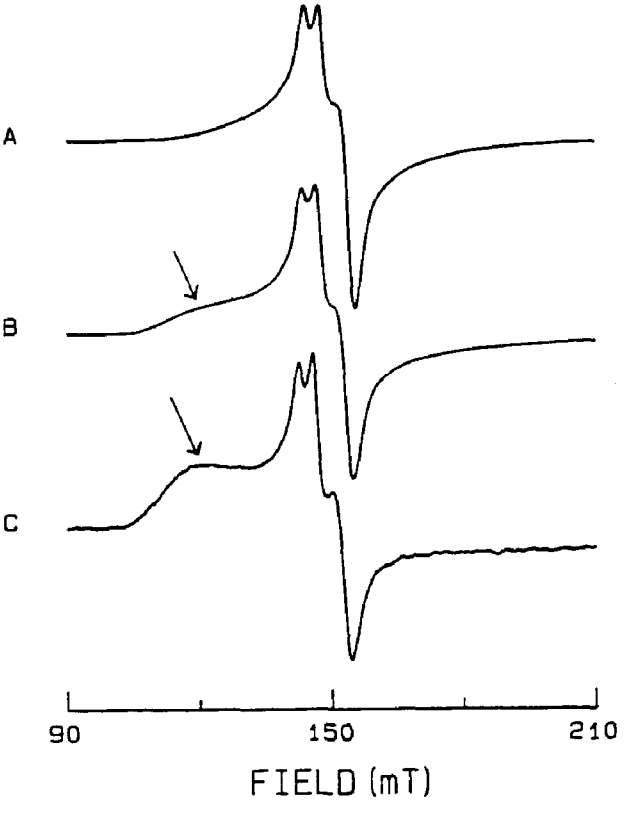

Figure 2.4 The effect of thiocyanate. Spectrum A is diferric transferrin, B is diferric transferrin and 0.33 M NaSCN, and C is diferric transferrin, 0.26 M NaSCN and 0.21 M NaCN. The arrow denotes shoulder induced by thiocyanate. Solution conditions: protein concentrations are 0.98 mM, 0.66 mM and 0.44 mM for A,B, and C, respectively, 90% iron saturated, pH 10.4. Instrument gain is 62 for A and 320 for B and C. Spectra are scaled to the same peak height. File 42A, 42D, and 42G, disc 1-86.

thiocyanate plus cyanide (Fig. 4C) on the g' = 4.3 EPR spectrum of diferric transferrin (Fig. 4A) are seen. Since the shoulder at 120 mT (Fig. 4B & C) appears to be associated with anion binding, in this case SCN^- binding, in the N-terminal domain of the protein (34), we conclude that the low spin cyanide adduct likely forms in the C-terminal domain. Such a conclusion is evident from Figure 4C in which the shoulder is much more pronounced because of loss of the signal contribution from the C-terminal site to the observed spectrum. The spectrum in Figure 4C has an integrated intensity approximately half that of spectrum 4B. The loss in intensity in the g'=4.3 spectrum is associated with a gain in the intensity of the g'= 2 spectrum (not shown).

The computer sum of spectra 4A and 4C, appropriately weighted to reflect 50% of the iron in each case, is shown in Figure 5A. Spectrum 5B is essentially the same as 4C, printed again for comparison. The close correspondence confirms the hypothesis of adduct formation occurring at only one site. Finally, equilibrium studies of bicarbonate and cyanide binding are consistent with this conclusion (vide infra).

Bicarbonate Dependence on Adduct Formation. Evidence for Replacement of Bicarbonate by Cyanide at the Iron Binding Site

As mentioned earlier, adduct formation was found to occur readily if excess bicarbonate was removed from

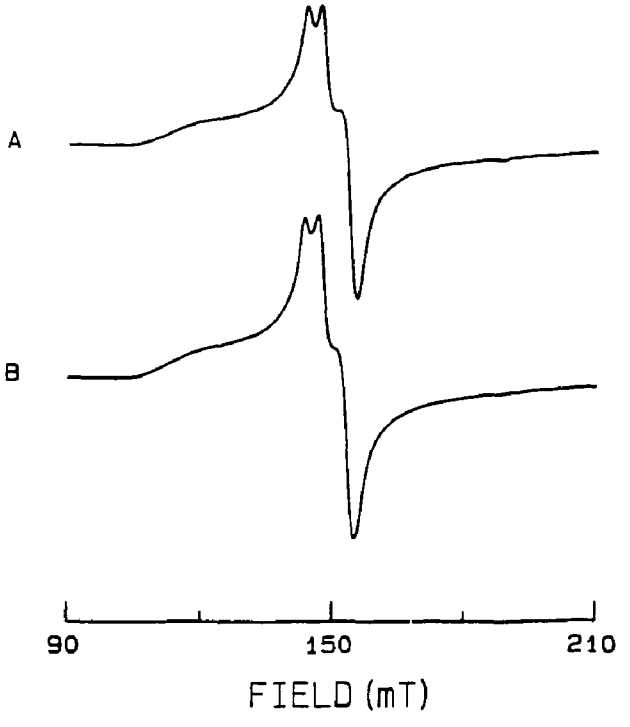

Figure 2.5 Computer addition of spectra from Figure 4. Spectrum A is the computer sum of A and C from Figure 4. Spectrum B is the same as B in Figure 4. File 42G.ADD, disc 1-86.

diferric transferrin solutions. In order to quantitate this effect, the extent of adduct formation was studied as a function of bicarbonate concentration. The general equation for formation of adduct is:

$$Fe\text{-}Tf\text{-}HCO_3 + nCN^- \longrightarrow Fe\text{-}Tf\text{-}(CN)_n + xHCO_3^-$$

where x = 0 indicates no bicarbonate displacement and x = 1 indicates one bicarbonate is displaced. The subscript n is the number of cyanides involved in the reaction.

The conditional equilibrium constant for adduct formation as a function of bicarbonate concentration can be written as:

$$K = [Fe\text{-}Tf\text{-}CN_n][HCO_3^-]^x/[Fe\text{-}Tf\text{-}HCO_3][CN^-]^n$$

A plot of the natural log of the $[Fe\text{-}Tf\text{-}HCO_3]/[Fe\text{-}Tf\text{-}(CN)_n]$ ratio as a function of the logarithm of the bicarbonate concentration will give a line which has a slope equal to x, the stoichiometric amount of bicarbonate replaced in the reaction. Such a plot is shown in Figure 6 where the concentration of cyanide was maintained at a constant value of 0.2 M. The slope is equal to 0.5 and appears to be non-linear in the higher concentration region. A slope of 0.5 suggests either that more than one protein molecule is involved in the overall bicarbonate reaction or, more likely, that only one site is involved in the equilibrium.

A second plot, assuming only one site on the protein is involved in adduct formation, is shown in Figure 7. Here the slope is approximately one with the data being linear over the range. The experiment was repeated, except the concentration of cyanide was held constant at 0.4 M. Again,

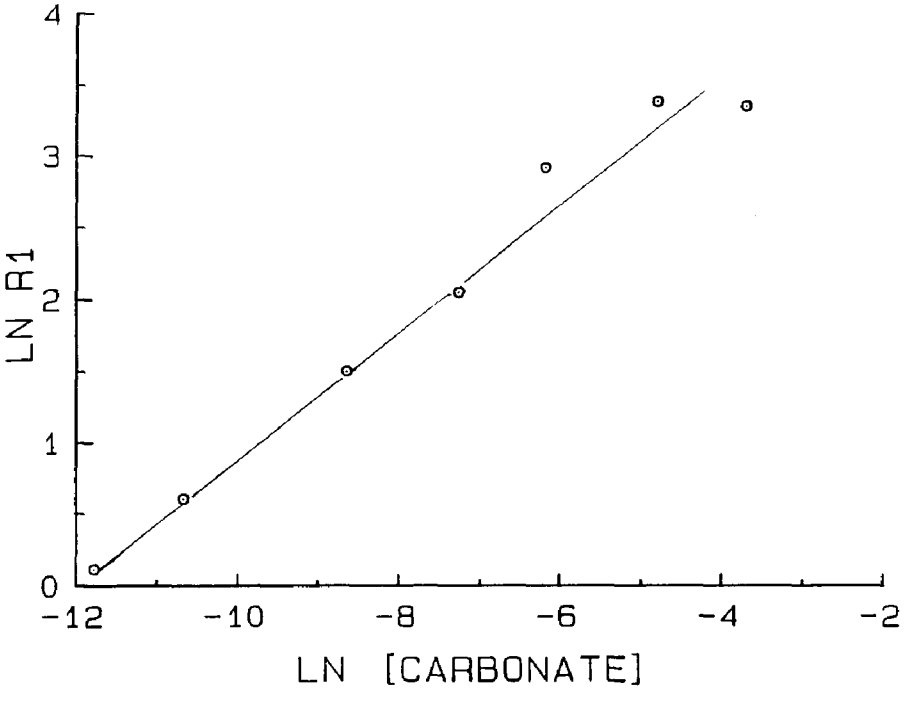

Figure 2.6 Natural log of the ratio of iron transferrin to adduct as a function of the natural log of concentration of carbonate (LN R1). Both sites are assumed to be involved in adduct formation. Conditions: 0.2 mM protein, 90% saturated, pH 10.6, 0.2 M NaCN. Linear regression slope = 0.43 +/- 0.08, correlation coefficient: 0.988. File CO32S.DAT, disc 6-86.

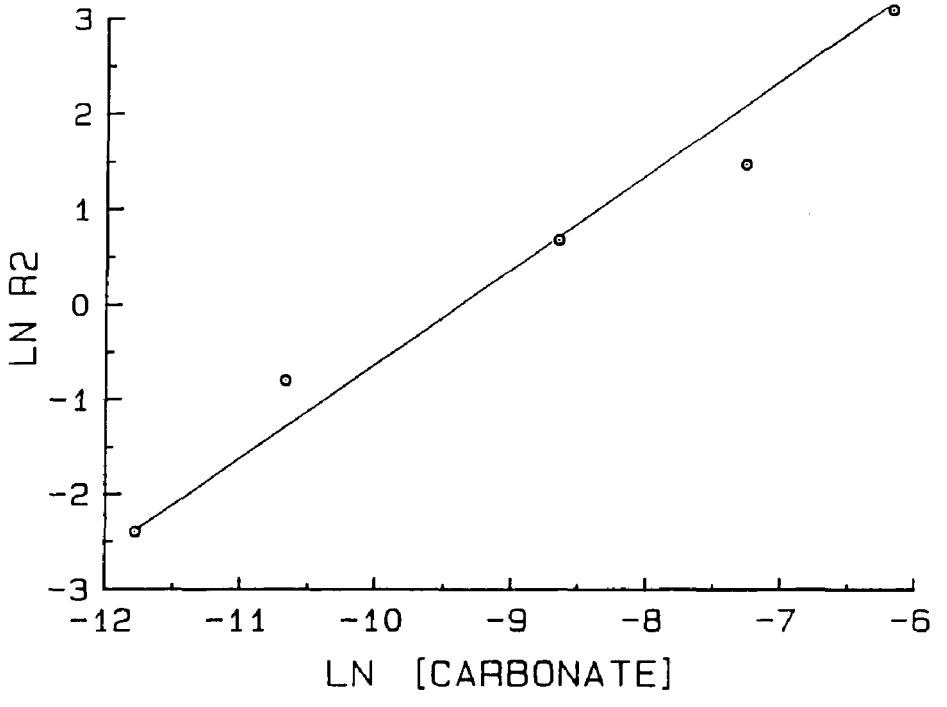

Figure 2.7 Same data as Figure 6, except R2 is the ratio assuming only one site is involved in adduct formation. Slope = 0.90 +/- 0.26, y-intercept = 8.4 +/- 2.3, correlation coefficient = 0.988. The conditional equilibrium constant, calculated from the y-intercept, assuming x = 1 and n = 3, is 0.31 M^{-2}. (The 95% probability range is between 0.14 and 0.67 M^{-2}.) File C031S, disc 6-86.

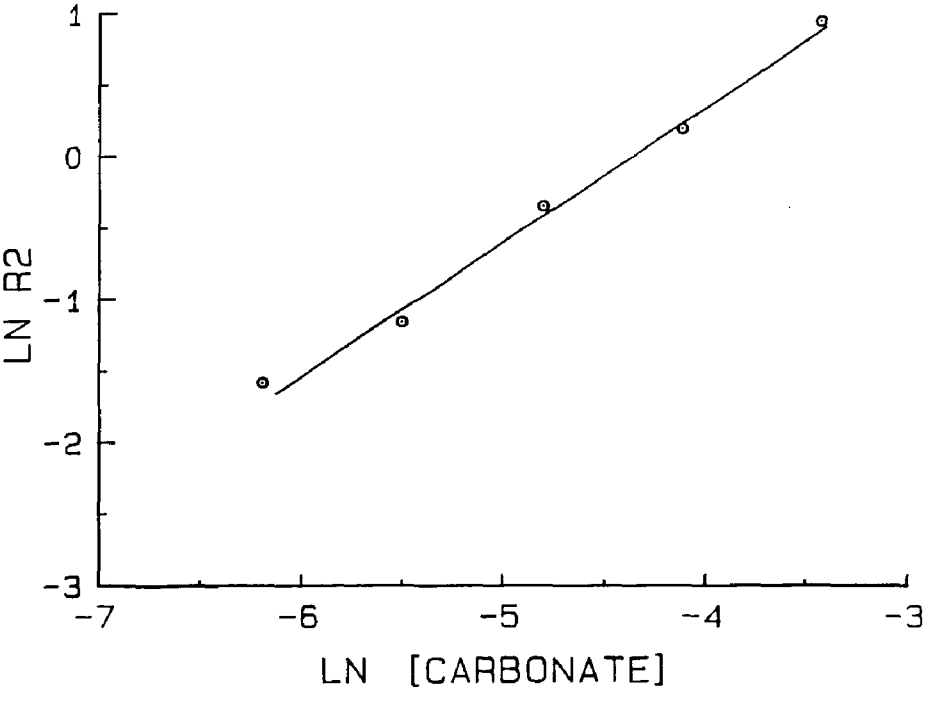

Figure 2.8 Natural log of the ratio of the concentration of diferric transferrin to adduct (LN R2) as a function of the natural log of carbonate concentration, assuming only one site involved in adduct formation. Conditions: 0.18 mM protein, 90% saturated, pH 11, 0.4 M NaCN. Slope = 1.09 +/- 0.14; correlation coefficient = 0.998. File 1225P2.DAT, disc 6-86.

a plot based upon only one site gave a slope of approximately one (Fig. 8). These data indicate that the synergistic anion bicarbonate (or carbonate) is being replaced during adduct formation.

From the data in Figure 7, the conditional equilibrium constant for the formation of adduct from native transferrin, is 0.31, for x = 1 and n = 3 (vide infra). The upper and lower limit, based on the 95% confidence interval of the y-intercept, is 0.67 and 0.14, respectively.

Cyanide Dependence on Adduct Formation.

For the invesigation of cyanide dependence, experiments were done in which the concentration of cyanide was varied in the presence of minimal concentration of bicarbonate at pH 10.4. A plot of the natural log of the ratio of adduct to iron transferrin as a function of the natural log of cyanide concentration, assuming only one site is involved in adduct formation, is shown in Figure 9. The value of n equals 3.01 +/- 0.20, suggesting that three cyanides are involved in formation of the low spin adduct signal. A plot assuming both sites are involved (not shown) gives a slope of 2.60 +/- 0.23.

In order to determine whether iron was being conserved during the titration, the double integrals were converted to iron concentration and the total iron was determined. The results shown in Table III indicate that within experimental error the iron is being conserved. The precision of double integrals of EPR spectra is typically 10-15%.

Table 2-III

TOTAL DOUBLE INTEGRAL OF LOW SPIN AND HIGH SPIN IRON AS A FUNCTION OF CYANIDE CONCENTRATION

Cyanide Concentration (mM)	Double* Integral g=4.3 region	Double* Integral g=2 region	Total Double Ingegral
40	11.88	0.16	12.04
60	11.18	0.29	11.47
80	11.24	0.45	11.69
100	10.43	0.73	11.16
167	9.30	1.96	11.26
200	8.07	3.35	11.42
250	8.01	4.26	12.27
300	7.17	5.48	12.65

* Normalized to the iron concentration using appropriate EPR standards. (See Materials and Methods section.)

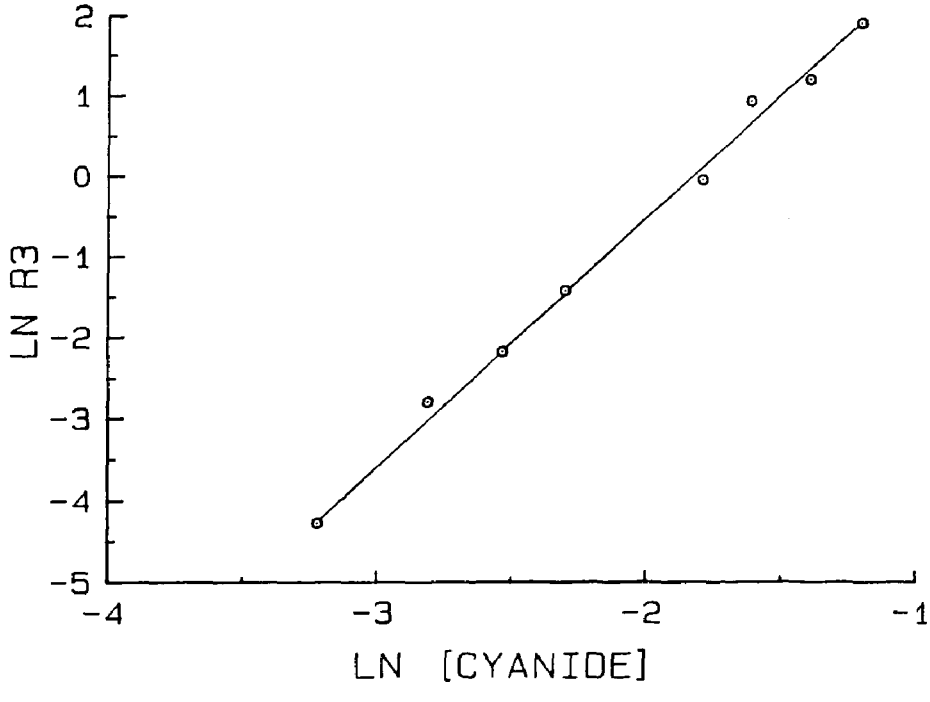

Figure 2.9 Natural log of the ratio of the concentration of adduct to diferric transferrin (LN R3) as a function of the log of the cyanide concentration, assuming only one site is involved in adduct formation. Conditions: 0.50 mM protein, 90% saturated, pH 10.4. Slope = 3.01 +/- 0.20; Correlation coefficient = 0.998. File CN1S.DAT, disc 6-86.

Kinetic Effects on the Equilibrium Between High Spin and Low Spin Forms of Transferrin.

Although no attempts were made to measure rate constants or to determine the mechanism of the formation of the low spin adduct, some important observations related to the kinetics of this reaction were obtained. First, low spin iron(III) complexes are kinetically inert (67). Thus, in our experiments, it was not possible to reverse the reaction once formation of adduct had occurred. In the equilibrium studies, it was therefore only possible to approach the equilibrium from one direction, i.e. adduct formation.

The production of low spin adduct from diferric transferrin was a relatively slow process, and in the course of the reaction the EPR spectra showed evidence for formation of a species with high spin axial symmetry (see Figure 10). In this experiment, cyanide was added to a solution of diferric transferrin, and the sample was frozen at intervals in EPR tubes; spectrum A is the sample within one minute after mixing, spectrum B that 20 minutes after mixing, and spectrum C that 60 minutes after mixing. The samples were developed at room temperature.

Spectrum A shows evidence for an intermediate complex that presumably is generated in the course of adduct formation. The complex appears to have greater axial symmetry than native transferrin and exhibits a spectrum similar to that when either oxalate or malonate replaces

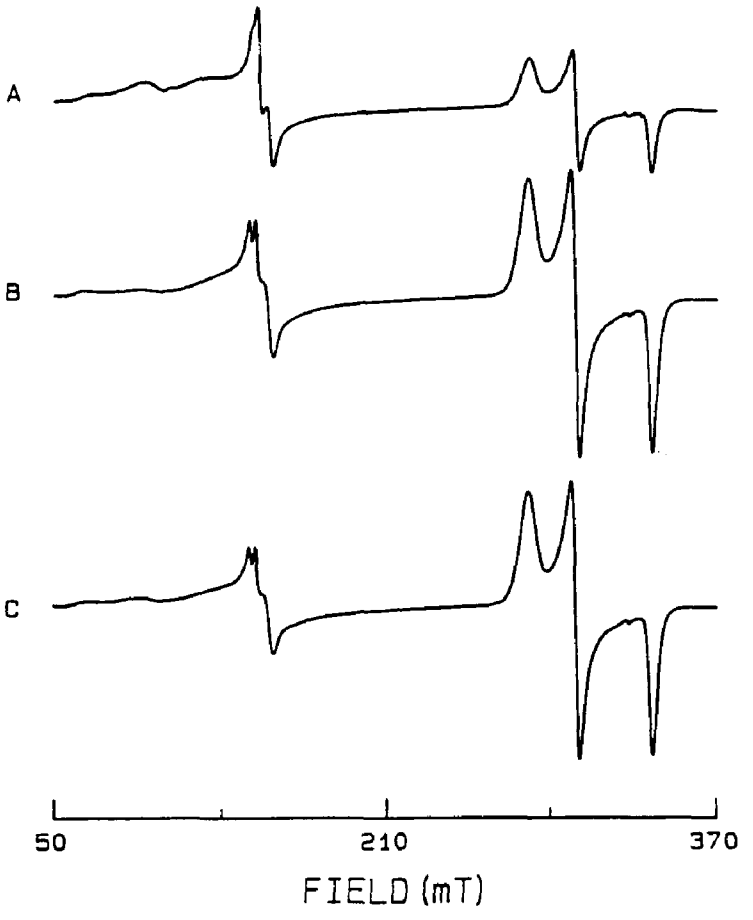

Figure 2.10 Time dependence for adduct formation. Spectrum A is within one minute after mixing, B is after 20 minutes at room temperature, and C is after 60 minutes at room temperature. Other solution conditions: [protein] = 0.58 mM, 90% saturated, 0.7 M NaCN, pH = 11. Receiver gain is 620 for A and B and 500 for C. File CNP7M, CNP7MP, and CNP7X, disc 11-85.

Table 2-IV

TIME DEPENDENCE FOR ADDUCT FORMATION
(see Figure 10)

Development Time	% high spin*	% low spin*
< one minute	81%	19%
20 minutes	53%	47%
60 minutes	53%	47%

*As determined by double integral (see Methods).

bicarbonate in the iron binding site of transferrin (see reference 26). Double integrals taken of the EPR spectra A-C indicate that all of the iron remains EPR active over the course of the reaction (see Table IV). However, in spectrum A, only 19% of the iron is low spin, while in spectra B and C, the conversion to low spin iron appears to be complete with 47% of the iron in the low spin form. However, the peak height of the transferrin signal in the 60 minute spectrum has descreased slightly in this time period.

Coordination Complexes Which Exhibit Low Spin Iron(III) EPR Signals Similar to the Adduct Signal

EPR spectra of Fe(EDTA), $Fe(NTA)_2$, and $FeCl_3$ in the presence of 1 M cyanide at pH 10.5 were measured; all give low spin rhombic signals with similar g values (see Figure 11 and Table V). It is possible to distinguish the Fe(EDTA) complex from the other three species on the basis of g-values. It also is evident that the lineshapes of the signals of the low molecular weight complexes differ from that of the adduct.

It is not known whether the iron remains coordinated to EDTA or NTA in these solutions. The high pH may affect the stability of these complexes. Because of HCN evolution and its toxic nature (pK_a 9.2), it was not possible to lower the pH appreciably.

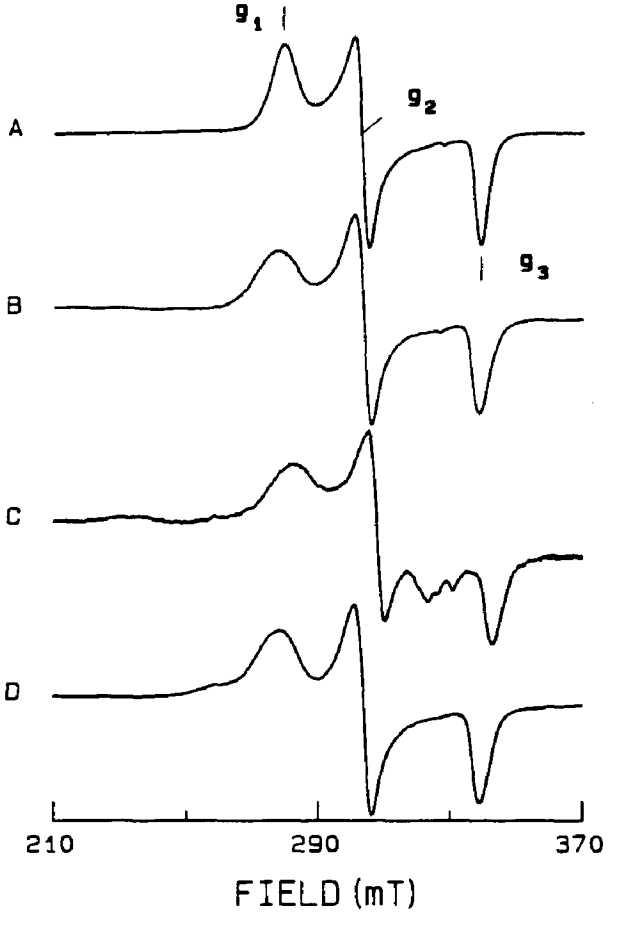

Figure 2-11 EPR spectra of low spin iron complexes: (A) diferric transferrin (from Fig. 2), (B) $FeCl_3$, (C) Fe(EDTA) and (D) $Fe(NTA)_2$. The corresponding g-values are tabulated in Table V. All samples are approximately 1mM in iron and 1mM in sodium cyanide, pH 10.5. Receiver gain is 400 for B-D. Files J23FEC, J23FEE, J23FEN, disc 11-85.

Table 2-V

G-VALUES OF LOW-SPIN COORDINATION COMPLEXES IN FIGURE 11

	g_1*	g_2	g_3
$FeCl_3$	2.36	2.18	1.95
Fe(EDTA)	2.33	2.14	1.93
$Fe(NTA)_2$	2.36	2.18	1.95

*The uncertainty in the g-values is approximately +/- 0.01.

Temperature Depencence of the Low Spin Adduct EPR Signal

The question of possible spin-crossover in the adduct sample was considered because of anomalous changes in the EPR spectra of adduct samples during storage. Typically, EPR samples of iron transferrin stored at temperatures below -100°C showed no change in their EPR spectrum over time. However, this was not always true for the adduct samples. For example, Figure 12A shows the EPR spectrum of a sample of approximately 0.5 mM diferric transferrin and 0.5 M cyanide at pH 11 frozen in dry-ice acetone after development for ten minutes at room temperature. The spectrum was measured immediately. Spectrum B is the same sample left overnight in dry-ice acetone at -95°C and measured again the next day. Significant changes in the spectrum occurred.

Literature on spin-crossover compounds indicates that temperature-related hysteresis effects as well as "abrupt" transitions and transitions which are incomplete on either the high temperature or low temperature end are often observed (68). The adduct signal was therefore measured as a function of temperature.

The Curie-Weiss law predicts that the EPR signal should be proportional to the inverse of the absolute temperature. Deviations from this behavior may indicate a change in the spin state of the species under study. In a preliminary experiment, the temperature dependence of the adduct sample was measured as a function of temperature from 77K to 233K (the sample showed evidence of local melting at 233K). The

shape of the spectrum as a function of temperature is shown in Figure 13, while Figure 14 shows a plot of the double integral as a function of 1/T. There appears to be a discontinuity in the 1/T plot, indicating that the adduct may be exhibiting spin crossover. Further work will be required to verify this result.

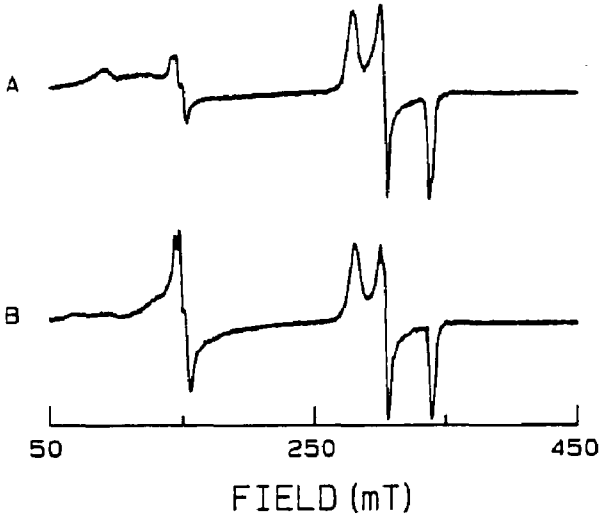

Figure 2.12 Changes in the EPR spectrum during storage at -100°C. A is a sample after freezing in dry ice/ acetone, and B is after overnight storage. Other conditions: 0.4 mM protein, 90% saturated, 0.5 M NaCN, pH 11. Instrument gain = 400. File 12123 and 12124, disc 6-86.

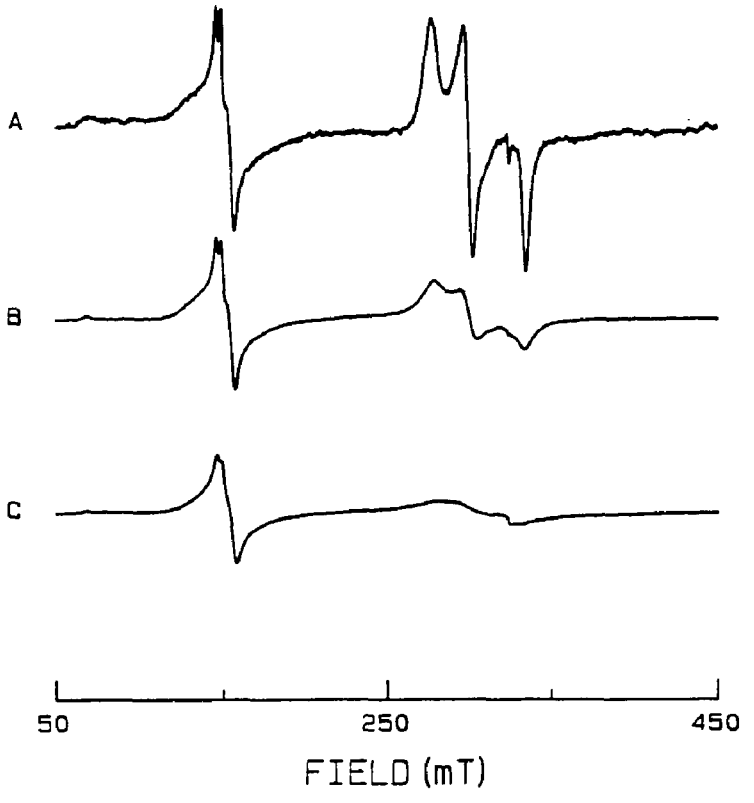

Figure 2.13 EPR spectra of samples of diferric transferrin (0.58 mM, 84% saturated) in 0.5 M NaCN, pH 10.5, at various temperatures. Spectra A, B, and C are taken at 93K, 153K, and 213K, respectively. Receiver gains are 2000, 2500 and 4000 for A,B and C, respectively. File LT7, LT4 and LT1, disc 4-86.

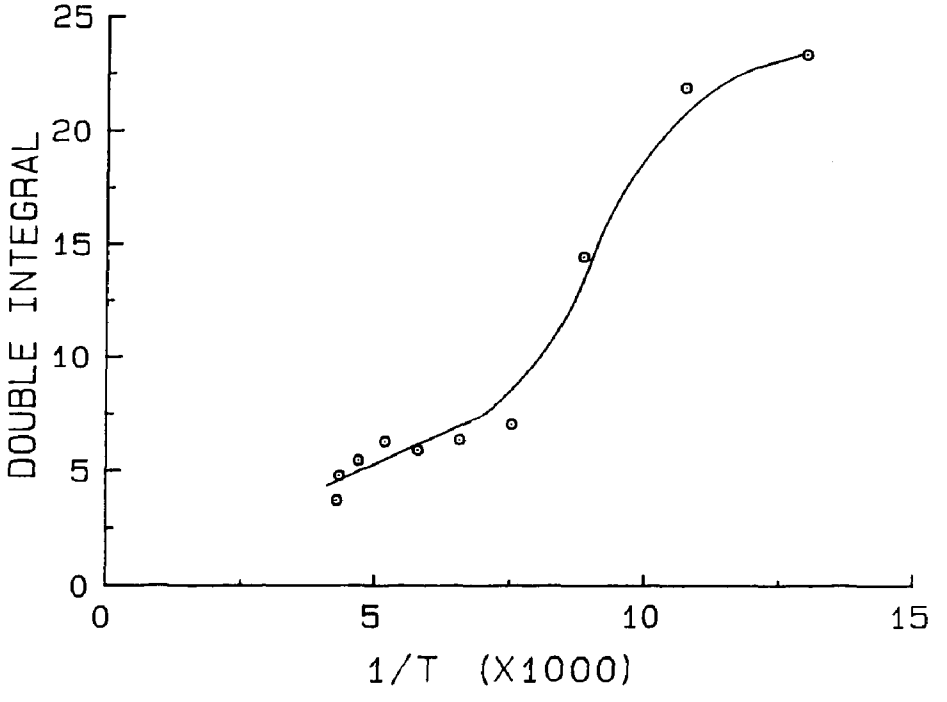

Figure 2.14 The total double integral as a function of the inverse of the absolute temperature. The sample is the same as Figure 13.

DISCUSSION

The equilibrium studies indicate the following stoichiometry for formation of the cyanide adduct of transferrin:

$$Fe_c\text{-}Tf\text{-}HCO_3 + 3\ CN^- \longrightarrow Fe_c\text{-}Tf\text{-}(CN)_3 + HCO_3^-$$

The subscript "c" denotes the C-terminal half of the protein. The most reasonable explanation of this stoichiometry is that at least one cyanide replaces the bicarbonate in the first coordination sphere of the metal. The other two cyanide molecules also could be coordinated to the metal. On the other hand, the two cyanides may bind at anion binding sites on the protein, causing a conformational change which leads to formation of the adduct. The fact that two anions may be involved in producing a conformational change is reasonable since certain anions such as perchlorate bind to the C-terminal domain of transferrin pairwise with positive cooperativity (33,34). It is not possible to distinguish between these two alternatives with the present data.

The replacement of bicarbonate by cyanide is an unexpected finding. Prior to this work, it was thought that in order for an anion to be an effective replacement for bicarbonate it had to possess a carboxyl group and thus be "bicarbonate-like" (30). In the absence of such an anion, it has been suggested that the protein loses its iron to non-specific binding and formation of hydrolytic Fe(III)

polymers (69). The present study appears to contradict this assumption.

It is likely that the synergistic anion plays a role in the exchange of iron with transferrin *in vivo* (3). However, the precise nature of this function is not known. Our results indicate that specifically bound iron is, under appropriate conditions, susceptible to attack by chelators (*i.e.* cyanide in this case) at the anion binding site. This suggests that, *in vivo*, biochelators may have accessibility to the iron binding site. A possible mechanism is thus suggested in which biochelators bind directly to the iron, possibly at the anion binding site, in the first step in the process of iron exchange.

Unfortunately, the g-values obtained for the adduct appear to be relatively insensitive to the coordination environment of the metal. The Schiff base complexes of iron and the adduct all have very similar g-values (see Table II, Figure 2, and Table V). Analysis suggests (58) that the unpaired electron for these complexes lies in the d_{xy} orbital, irrespective of the axial ligands. Thus, although axial coordination of the cyanide or other strong field ligands can force the compound to low spin, the corresponding g-values are insensitive to the details of the axial ligands.

It has recently been reported that 1:2 low spin complexes of iron(III) with sodium 2-pyridinecarboxaldehyde dithiocarbazonate, and related ligands, show promise as drugs for chelation therapy (70). In some cases, these

compounds have been shown to be more effective than desferrioxamine in the removal of iron from transferrin and ferritin. Desferrioxamine is a naturally occurring iron chelator that is commonly used in chelation therapy. It is interesting that the efficacy of these drugs derives in part from the kinetic inertness of their low spin complexes (71).

CHAPTER III

A STUDY OF THE ANION BINDING REGION OF TRANSFERRIN USING NITRATE BINDING AND N-15 NMR SPECTROSCOPY

INTRODUCTION

Amino acid string models of transferrin indicate that there are an unusually large number of cationic groups close to the iron binding region (8,13). It has been suggested that lysines or arginines which are in the vicinity of the iron function as specific binding sites for anions (34). One way to test this hypothesis is to estimate the anion-metal distance using NMR relaxation measurements.

Paramagnetic metal ions in the vicinity of relaxing nuclei can increase the rate of nuclear spin relaxation dramatically. Therefore, a nucleus of an anion binding at a site close to the paramagnetic iron(III) in transferrin may show increased relaxation. When "fast exchange" occurs between the anion and the protein, the bulk relaxation will be an average of the relaxation of bound and free anions (72). Under these conditions, a nucleus will show increased relaxation proportional to the inverse sixth power of the distance between the anion and iron binding sites.

The anion used in this study was nitrate, and N-15 NMR spectroscopy was used to measure the paramagnetic relaxation enhancement. N-15 NMR is inherently insensitive in signal to noise ratio, both because the magnetogyric ratio of the nitrogen-15 nucleus is small (approximately one tenth that of the proton) and because its natural abundance is low (0.36%) (73). In order to compensate for this disadvantage, enriched nitrate ($Na^{15}NO_3$) was used.

Furthermore, the N-15 nucleus is characterized by slow

relaxation with spin lattice relaxation times (T_1) often exceeding 100 seconds (74). For this study, the relaxation characteristics present a tradeoff. Because the relaxation time is long, it has the potential for great sensitivity to increased relaxation enhancement by the paramagnetic iron. However, slow relaxation times require long data acquisition times.

MATERIALS AND METHODS

Because it is essential to remove any trace of metal from the solutions used for relaxation measurements, all glassware was soaked overnight in 50% HCl and rinsed thoroughly prior to use. All other solutions were shaken over Chelex 100 for at least 24 hours before use. The transferrin was dialyzed to remove any impurities by dissolving 500 mg of apotransferrin (Calbiochem) in 10ml of doubly deionized water. This solution was placed in a pre-rinsed dialysis bag (Spectrapor #1, 6000-8000 MW cutoff) and dialyzed for 8 hours at 4°C against three one-liter portions each of 0.15M $NaClO_4$, 2 mM Hepes (pH 6.8), and 2 mM Hepes, (pH 6.8). Sodium nitrate - 15N (99%) was obtained from Stohler/KOR Stable Isotope.

All NMR relaxation measurements were done on a JEOL FX 90Q NMR spectrometer; the nitrogen resonance frequency is 9.04 MHz. NMR tubes (10 mm diameter) fitted with vortex plugs were used for all measurements; typical sample volumes were 1.2 ml. For variable temperature experiments, the

temperature was measured using a copper constantan thermocouple inserted into a sample after it had reached equilibration in the NMR probe. The temperature readings were taken when the sample was not spinning. The temperature in the probe area was assumed to be a constant of 28 +/- 2 ^{o}C in other experiments.

T_1 measurements were made using either the inversion recovery method or the progressive saturation method (75). The 90^{o} pulse was determined before each T_1 measurement and found to be typically 60-64 us. The phase error detection method (76) was used either on the sample to be measured in a 10 mm tube or on a sample of 2M $NaNO_3$ in either a 5 mm or a 10 mm sample tube. When the 5 mm sample tube was used, the sample was inserted coaxially into the 10 mm probe, using special teflon holders.

The phase error detection method requires that the phasing first be set using a normal single pulse acquisition with a pulse width less that ninety degrees. Then, a (180 - t - 90) sequence is applied, using a very short t (.05 s) while varying the pulse width for the 180^{o} and 90^{o} pulses. When the test value is the true 90^{o} pulse, the spectrum will be completely inverted and properly phased.

The inversion recovery method for T_1 determination involves the following pulse sequence: $(180 - t - 90 - A_t - D)_n$, where t is the pulse interval between the 180^{o} and 90^{o} pulses, A_t is the acquisition time, and D is the time between the end of the acquisition time and the beginning of

the next pulse. Values for D were chosen such that (A_t + D) > 5 T_1 and values for t were chosen to span the range from approximately 0.4 T_1 to 1.2 T_1. The variable n is the number of transients used for the FID. The value of n was chosen such that a satisfactory signal could be obtained; typically, n = 20. The appropriate equation for the T_1 measurement is:

$$I_t = I_\infty [1 - 2\exp(-t/T_1)]$$

where I_∞ is the signal height measured at t = ∞, i.e. t is greater than 5-10 T_1's and I_t is the signal height at time t.

The pulse sequence used for the progressive saturation method can be represented as $(90 - A_t - D)_3 (90 - A_t - D)_n$. In this sequence, t, which ideally goes from .4 T_1 to 1.2 T_1, is the sum of the acquisition time A_t and the pulse delay D. The first three pulses are used to establish a stationary state where the rate of excitation and relaxation are approximately equal. Then, acquisition is begun and continues as usual. The appropriate equation for calculation of T_1 is:

$$I_t = I_\infty [1 - \exp(-t/T_1)]$$

The advantage of using the progressive saturation method is that it saves time compared to the inversion recovery method. Typically, a progressive saturation T_1 measurement can be done in 1/3 to 1/2 the time of an inversion recovery experiment. For measurement of a long T_1 (100 s), the measurement takes 9 hours by progressive saturation versus 27 hours using inversion recovery. The

disadvantage of the progressive saturation method is that it is sensitive to the accuracy of the 90^{o} pulse. The 90^{o} pulse must therefore be determined carefully.

The frequency width for all spectra was 50 Hz, and a maximum of 16K data points were collected. $A_t = N/2F$, where N is the number of array points collected and F is the frequency width. Therefore, the aquisition time equals 163 seconds when all 16K array points were collected.

Typically, some zero filling was necessary in order to decrease the acquistion time to a reasonable level. A requirement for use of the progressive saturation method is that, for long T_1's, T_2^* must be much less than T_1, where T_2^* is the effective transverse relaxation time. This criterion is satisfied in our case, as evidenced by the decay of the FID. Thus, it is possible to zero-fill in order to satisfy the criteria that (A_t + D) be between 0.4 and 1.2 of the estimated T_1. For example, for a T_1 estimated to be 20 s, the (A_t + D) should be 8 s for the shortest interval. Thus, N = 800, and the remaining array points are zero filled. For a particular T_1 determination, the amount of zero filling was kept constant. This technique did not result in any noticeable change in the transformed spectra since the FID had decayed away by the time zero filling was begun.

Approximately 20 transients (n) were taken for each point on the T_1 graph, and 7 signals (the maximum number that could be stored on a floppy disc) were measured for

each T_1 measurement . Usually, the first and last measurements taken were the infinity values, since accuracy here was essential for the T_1 calculation. Furthermore, since some T_1 measurements took as long as a day, it was important to determine whether the instrument had been stable over this time period.

All spectra were stored on floppy disc using the automatic STACK pattern. Analysis of the data for T_1 measurement was done on the computer attached to the spectrometer, using the JEOL packaged program. When doing calculations involving the saturation recovery method, the appropriate calculation option must be chosen.

Procedures for EPR measurements and details of the electrophoresis technique are described in Chapter 1.

RESULTS

EPR Evidence for Nitrate Binding to Transferrin

Binding of anions to diferric transferrin is often indicated by perturbations in the EPR spectrum (33). Figure 1A shows the EPR spectrum of diferric transferrin in the presence of 0.2 M $NaNO_3$; compared to the same sample in the absence of nitrate (1B), slight changes are evident. The strength of the interaction of different anions with transferrin (i.e. concentration dependence of the perturbation) has been shown to follow the lyotropic series (33). Nitrate has a position close to chloride in the series. Since maximum perturbation for chloride does not occur until the concentration is approximately 0.5 M, it is expected that the perturbation of the spectrum would be more dramatic at higher nitrate concentration.

Temperature Dependence of the Paramagnetic Relaxation

In order to obtain structural information from NMR relaxation data, it is first necessary to verify that the measured relaxation is not being affected by exchange (4). This can be done by measuring the paramagnetic contribution to the measured spin-lattice relaxation time (T_{1p}) as a function of temperature. A negative temperature dependence of the rate ($1/T_{1p}$) indicates that exchange effects are negligible (4).

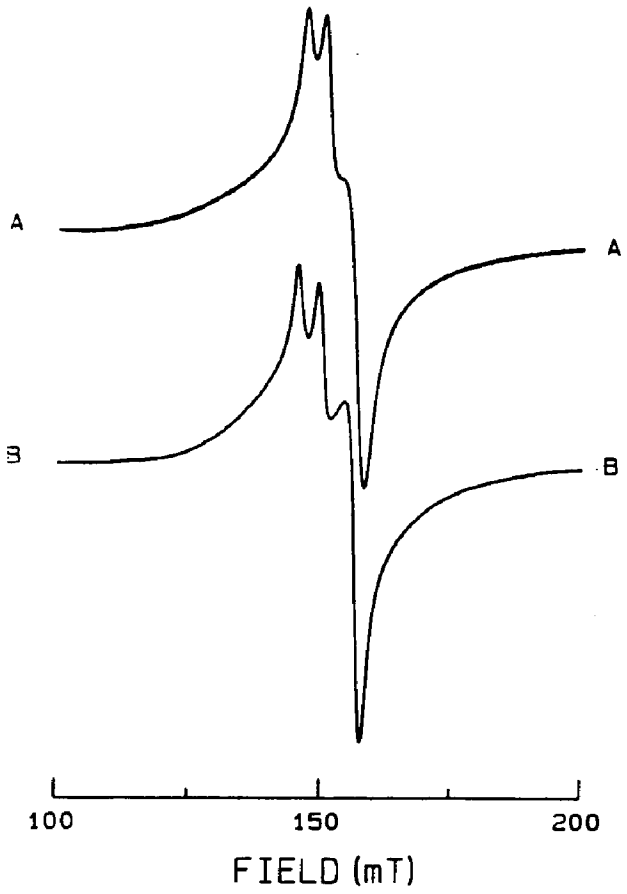

Figure 3.1 Comparison of the EPR spectra of diferric transferrin in the presence of 0.2 M sodium nitrate (A), and (B) in the absence of nitrate. Other solution conditions: 100mM Hepes, 20mM sodium bicarbonate, pH 7.4. Instrument settings: power = 20mW, scan time = 16 min/ 2000 G, field set = 1500 G, time constant = 1.0 s, modulation amplitude = 10 G, modulation frequency = 100 kHz, microwave frequency = 9.11 GHz. File FEN03, Disc 1 and File 16HR, Disc 10C.

The paramagnetic contribution to the spin-lattice relaxation rate is given by:

$$1/T_{1p} = (1/T_1)_{obs} - (1/T_1)_o$$

where $(1/T_1)_{obs}$ is the relaxation rate measured in the presence of diferric transferrin and $(1/T_1)_o$ is the relaxation measured with the apoprotein.* A plot of $(1/T_{1p})$ *versus* 1/T has a positive slope, indicating that exchange effects are unimportant in the relaxation (Figure 2) (72).

From an Arrhenius plot of the data (Figure 3), the activation energy for the process is approximately 2 kcal/mol, indicating that either the electron spin correlation time (τ_s) or the rotational correlation time (τ_r) is dominant. When τ_M, the length of time the nucleus spends in the sphere of influence of the paramagnetic iron, is dominant, the activation energy is in the range of 6-25 kcal/mol (72).

* Rigorously, $(1/T_1)_o$ should have been measured in the presence of a Co(III) transferrin derivative, rather than the apoprotein. In the case of binding of the diamagnetic metal, the tertiary structure of the protein would be similar, if not identical, to that of diferric transferrin. This could affect the rotational correlation time, as well as provide different sites for anion binding. However, studies done on proton relaxation in the presence of apotransferrin and Co(III) bound transferrin suggest that the difference in T_1 would be small (77). Furthermore, the linearity in our plots for determination of T_{1M} (vide infra, Figures 6 & 7) suggests that the difference between the relaxation time measured in the presence of the cobalt derivative *versus* that obtained for the apoprotein is insignificant.

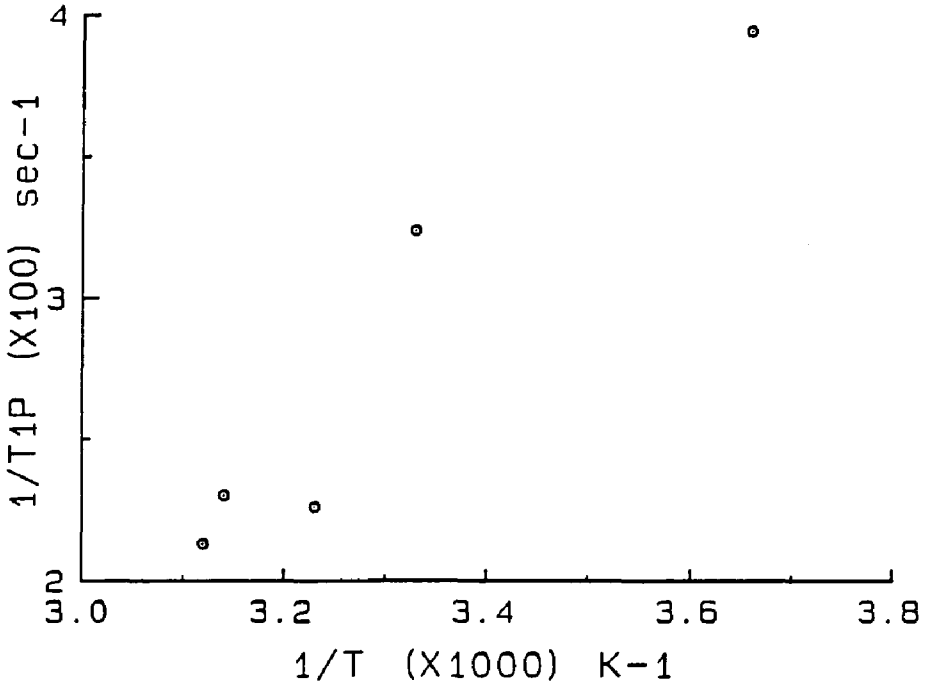

Figure 3.2 Plot of the paramagnetic contribution to the spin-lattice relaxation rate as a function of the inverse of the absolute temperature. Conditions: 0.355mM transferrin, 0.639 mM Fe (90% Fe saturated protein), 100 mM Hepes, 20 mM sodium bicarbonate, 0.2 M sodium nitrate, pH 7.4, 10% deuterium oxide.
(File 051685, Disc 6-86.)

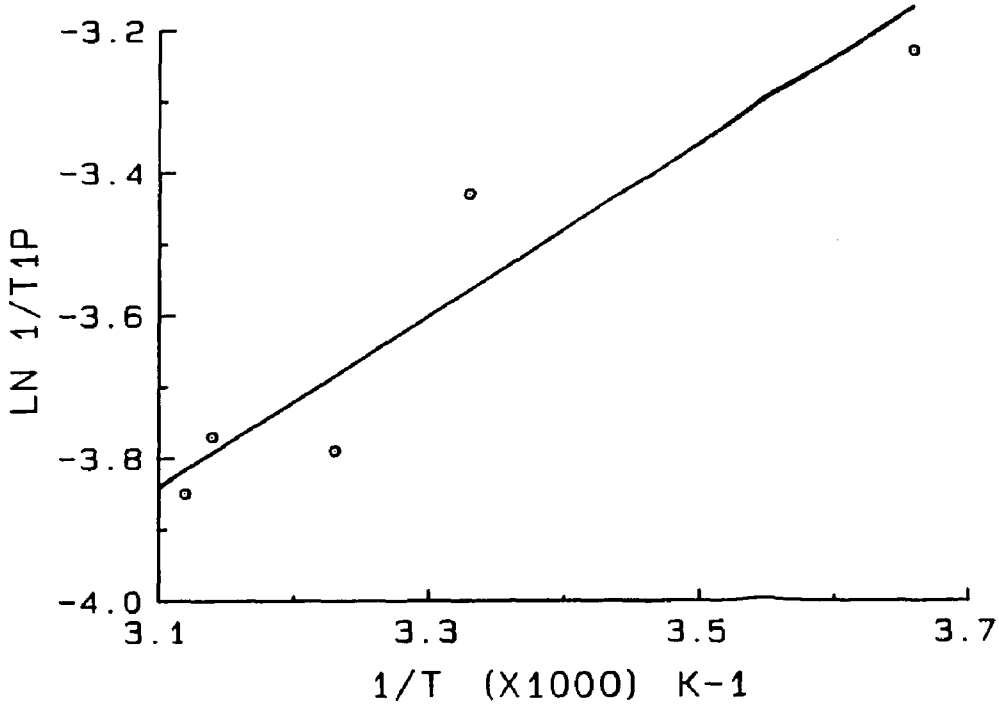

Figure 3.3 Plot of ln ($1/T_{1P}$) vs. 1/T. Conditions the same as in Figure 2. Slope is E_a/R; linear regression gives E_a = 2.30 +/- 1.53 kcal/mol, correlation coefficent 0.94. (File 51685G, Disc 6-86.)

Paramagnetic Relaxation as a Function of the Ratio of Iron to Apotransferrin. Electrophoresis Results.

In order to verify that the relaxation effects were resulting from iron at the specific iron binding site, T_{1p} was measured as iron was titrated into a solution of apoprotein in the presence of 0.2 M $NaNO_3$. The data, shown in Figures 4 and 5, are the results of two different titration experiments. The break at a molar ratio of 2:1 indicates that the enhanced relaxation observed in the solution is a result of the iron at the specific binding sites of transferrin.

In order to determine whether iron was adding preferentially to one site on transferrin, samples of apotransferrin in which iron was added to the protein in varying molar ratios were prepared in the presence of 0.2 M $NaNO_3$. The four species of transferrin were separated and quantitated using urea-polyacrylamide electrophoresis (19). The results are summarized in Table I.

It appears that in the initial low molar ratio of iron to transferrin (0.5:1), iron adds nearly equally to both sites. Beyond this point, iron adds preferentially to the N-site in a 2:1 ratio. The calculated percent saturation was less than the molar ratio of iron added, suggesting that quantitative addition of iron is not occurring in the presence of nitrate. It is possible that insufficient time was allowed for complete iron binding in the electrophoresis experiment. Samples were developed for at

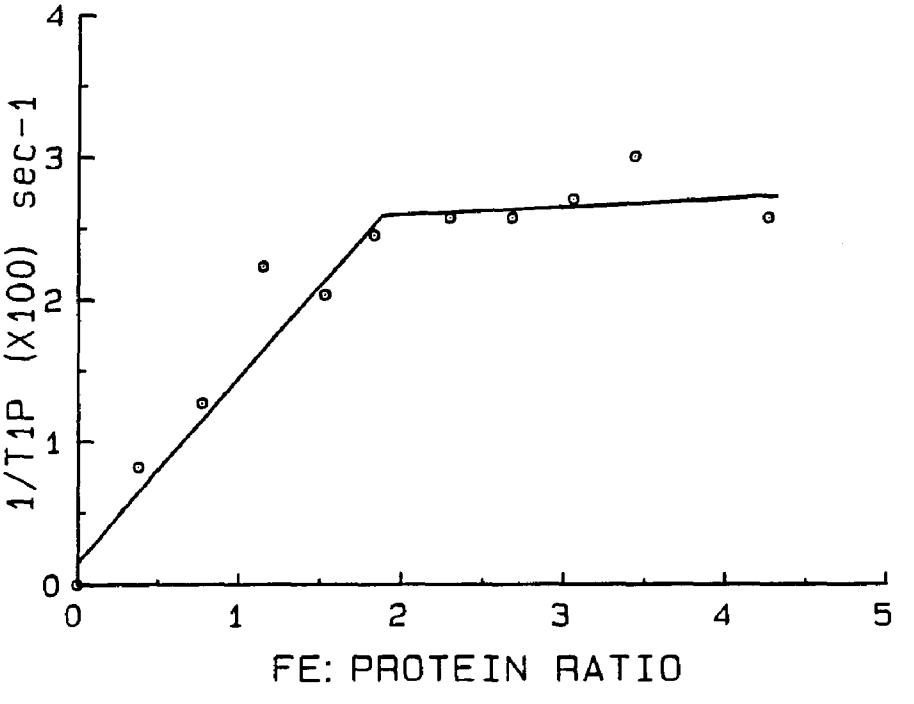

Figure 3.4 Plot of $1/T_{1P}$ vs. the iron to apotransferrin ratio. Conditions: 0.248mM protein, 100mM Hepes, 20mM $NaHCO_3$, 0.2M $NaNO_3$, pH 7.4, 10% D_2O. (File 052285, Disc 6-86).

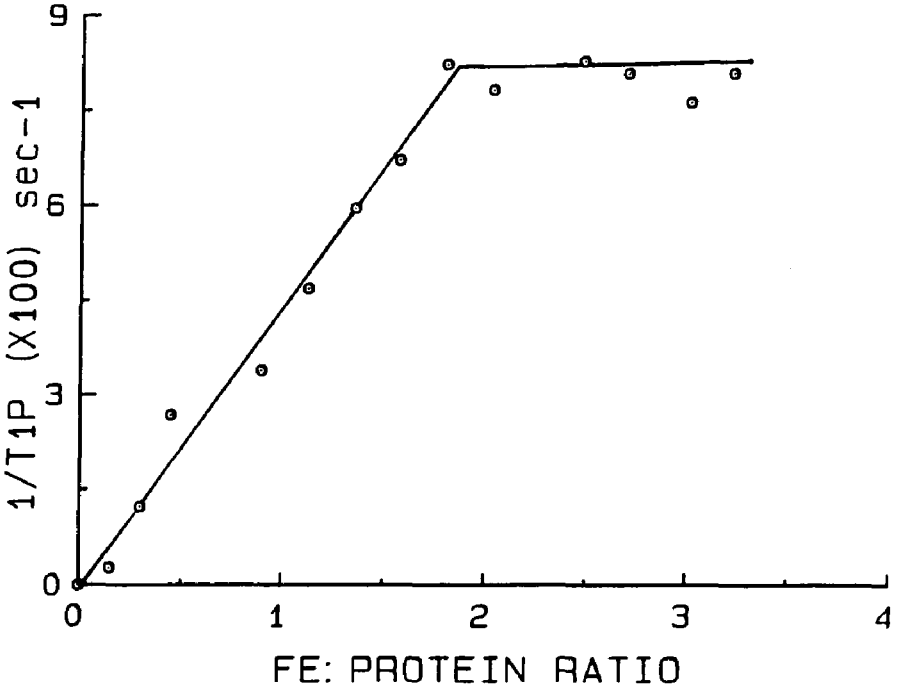

Figure 3.5 Plot of $1/T_{1p}$ vs. the iron to apotransferrin ratio. Conditions: 0.884 mM protein, 100 mM Hepes, 20mM $NaHCO_3$, 0.191M $NaNO_3$, pH 7.4, 10% D_2O. (File 102785, Disc 6-86).

TABLE 3-I

The Distribution of Iron in Transferrin in the Presence of 0.2M $NaNO_3$ as a Function of the Molar Ratio of Iron Added

Molar Ratio: (Fe:Apo)	0.5:1	1:1	1.5:1
Apotransferrin	52%	34%	24%
C-terminal	15%	16%	15%
N-terminal	22%	32%	35%
Diferric	11%	18%	26%
% Saturation*	30%	41%	52%

*Caculated from %saturation = (N + C + 2D)/2, where N, C, and D are the percent of the total integrated area that is N-terminal, C-terminal, and diferric, respectively.

least 2 hours, however; maximum saturation achievable in this short time is usually only 75%.

Determination of T_{1M}

In the case where the concentration of free ligand is much greater than the concentration of bound ligand, and exchange is not contributing to the relaxation, the following relationship holds (72):

$$1/T_{1p} = (1/T_{1M})n[Fe]/[NO_3^-]$$

where T_{1M} is the spin lattice relaxation time for nitrate bound to the protein at the anion binding site, [Fe] is the concentration of iron at the specific iron binding sites, and n is the stoichiometry of anion binding per iron.

Figures 6 and 7 are plots of the paramagnetic contribution to the spin-lattice relaxation rate vs. $[Fe]/[NO_3^-]$; the slope of the line equals (n/T_{1M}). For the first set of data (Figure 6), the slope equals 10.4 +/- 2.0 s^{-1}; for the second set of data (Figure 7), the slope equals 9.4 +/- .6 s^{-1}. Table I is a summary of T_{1M} for some possible values of n, calculated from the slope of the curve in Figure 7.

If a single anion binding site in only one of the iron binding domains causes the observed relaxation enhancement, then n = 0.5. On the other hand, an n value of 1 corresponds to one anion binding site in each domain. The titration data show a linear increase in $1/T_{1p}$. Since the electrophoresis data indicate iron(III) binds preferentially to the N-terminal site followed by the C-terminal site, it

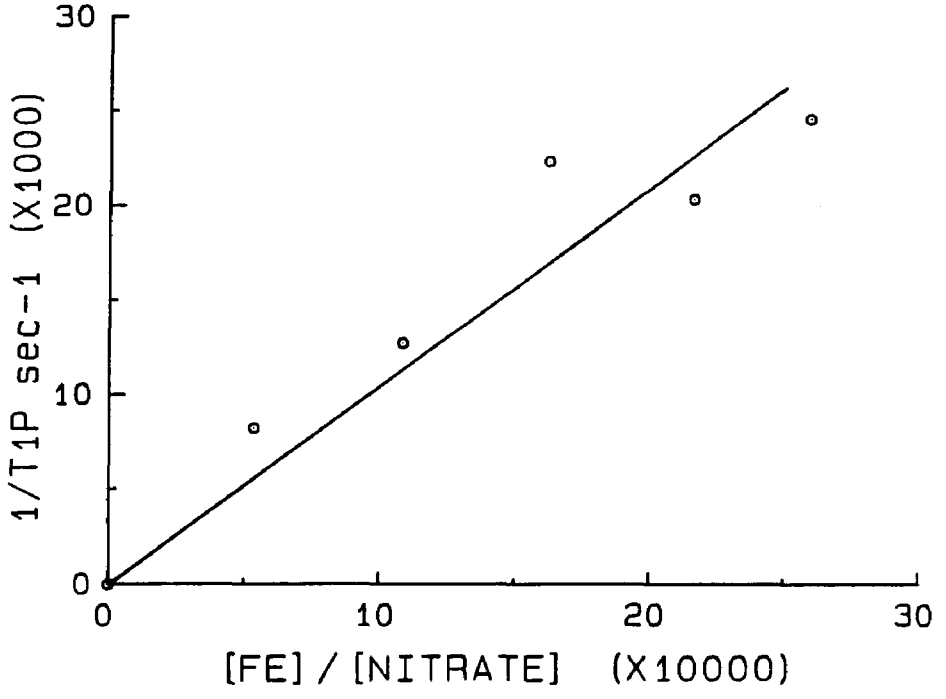

Figure 3.6 Plot of the inverse of T_{1p} versus the [Fe]:[NO_3^{-1}] ratio. The slope is 10.4 +/- 2.0 s^{-1}; correlation coefficient is 0.956. Data is calculated from Figure 4, where only points prior to the 2:1 ratio were used. File 516T1M, Disc 6-86.

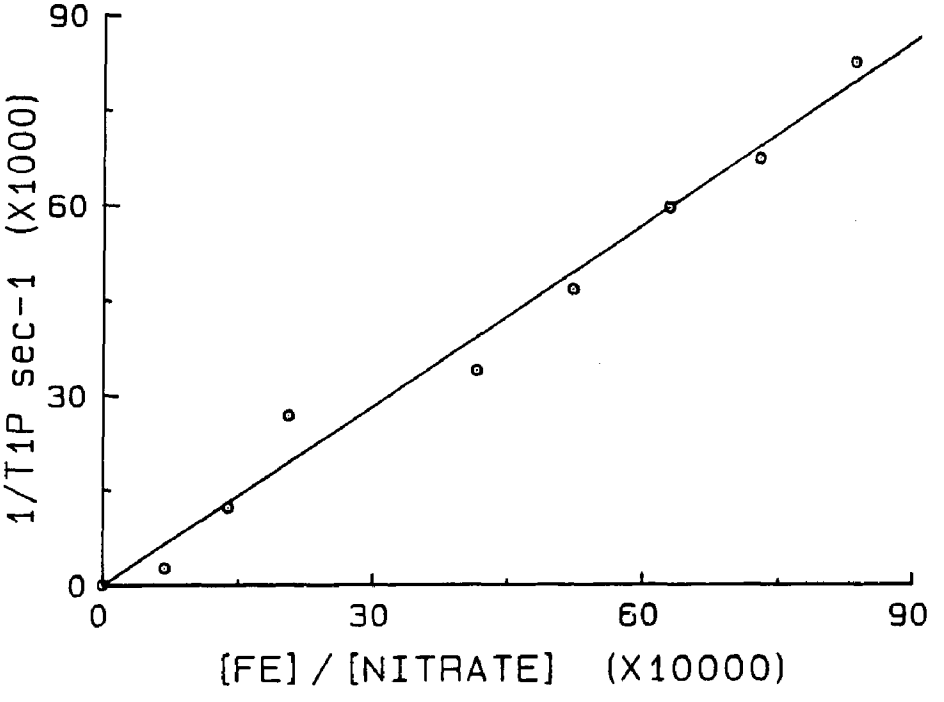

Figure 3.7 Plot of $1/T_{1P}$ vs. the [Fe] to [nitrate] ratio. The slope is 9.4 +/- 0.6 s^{-1}; the correlation coefficient is 0.991. Data is calculated from Figure 5. Only points prior to the 2:1 Fe:protein ratio were used. File 125T1M, Disc 6-86.

Table 3-II

The Spin-lattice Relaxation for the Nitrate Bound at the Anion Binding Site for Various Values of n

n	T_{1M}(s)
0.5	0.053
1	0.106
2	0.212

appears that both domains are involved in the relaxation enhancement and therefore that n is an integer.

Determination of the Distance of the Anion Binding Site from the Metal Binding Site

The Solomon-Bloembergen equation describes the paramagnetic contribution to the spin lattice relaxation time as a function of frequency, correlation time, and distance of the anion from the metal (72). The full equation includes two terms, one for the dipolar contribution and one for the scalar contribution. For dipolar contributions only, the relationship between T_{1M} and distance from the paramagnetic center is given by:

$$1/T_{1M} = 2/15\{S(S+1)\}\gamma^2 g^2 \beta^2 (1/r^6) Z$$

where

$$Z = 3\tau_c/(1+\omega_I^2\tau_c^2) + 7\tau_c/(1+\omega_s^2\tau_c^2)$$

and S (= 5/2) is the electron spin for iron, γ is the magnetogyric ratio for N-15, g is the electron g factor (=2.00), β is the Bohr magneton, ω_I (9×10^6 s^{-1}) is the Larmour precession frequency for the N-15 nucleus, ω_s (6×10^{10} s^{-1}) is the precession frequency for the electron, r is the metal-anion distance and τ_c is the correlation time. If we assume that $\tau_c = \tau_r = 23\times10^{-9}$ s-rad^{-1} (78), then $\omega_s^2\tau_c^2 >> 1$ and the equation simplifies to:

$$1/T_{1M} = 2/5\{S(S+1)\}\gamma^2 g^2 \beta^2 \tau_c (1/r^6) Z$$

where $Z = [1/(1 + \omega_I^2\tau_c^2)]$

The correlation time is given by:

$$1/\tau_c = 1/\tau_r + 1/\tau_s + 1/\tau_M$$

The temperature dependent data indicate that τ_M cannot be the dominant relaxation process because the activation energy is too low (72). From EPR linewidth measurements on vanadyl labelled transferrin, the rotational correlation time, τ_r, for the protein has been determined to be 23 x 10^{-9} s-rad^{-1} (78). A lower limit for the electron spin-lattice relaxation has been obtained from the linewidth of the room temperature EPR spectrum of iron transferrin, i.e. $\tau_s >= 3x10^{-10}$ s-rad^{-1} (77)*. In Table III, calculated anion-metal distances for various choices of n and τ_c are tabulated.

*The units of τ are usually reported in the literature as seconds (s), rather than s-rad^{-1} or s-cycle^{-1}. Since these differ by a factor of 2π, it is necessary to clarify this ambiguity. Generally, it seems that s-rad^{-1} are the appropriate units. See reference 79, page 9 and reference 80, Figure 1.

Table 3-III

Metal-anion Distance as a Function of the Stoichiometry of Nitrate Binding (n) and the Correlation Time (τ_c)

	n=0.5	n=1	n=2
$\tau_c = \tau_r \approx 23 \times 10^{-9}$ s-rad^{-1}	12.4 Å	13.9 Å	15.6 Å
$\tau_c = \tau_s > \approx 3 \times 10^{-10}$ s-rad^{-1}	7.2 Å	8.1 Å	9.1 Å

DISCUSSION

The electron spin relaxation time depends on frequency, temperature, and the ligands surrounding the metal. From EPR, we have a lower limit for τ_s obtained for iron in transferrin at room temperature, but at a lower magnetic field (0.15 Tesla) compared to NMR and therefore a corresponding lower frequency. Generally, τ_s makes a smaller contribution to the relaxation at higher frequencies (79), and so τ_s remains a lower limit.

The rotational correlation time obtained from vanadyl transferrin is an accurate value, and provides a reliable upper limit on the distance calculation. This is the case regardless of the accuracy of τ_s, because, if τ_s is actually greater than τ_r, τ_r will determine the overall correlation time.

In order to specify the precise anion-metal distance, it would be necessary to measure T_{1p} as a function of frequency. If the proper frequency range were available, this information would allow us to determine the appropriate correlation time to a higher degree of certainty. However, at this point, we can only conclude that the anion site is within 15 Å of the metal binding site, but farther than 8 Å. This leads us to conclude that positively charged amino acids in the immediate iron binding region remain likely candidates for the specific anion binding site(s).

APPENDIX

SECTION I: CHARACTERIZATION OF A HIGH MOLECULAR WEIGHT COMPONENT IN COMMERCIAL APOTRANSFERRIN PREPARATIONS

In the course of routine purification of apotransferrin using gel permeation chromatography (GPC), there were indications that the protein was self-associating. This finding was pursued because of the interesting possibility of dynamic association between apotransferrin molecules. Figure A.1 (C) shows the elution profile of commercially prepared apotransferrin (Calbiochem-Behring), indicating the presence of a high molecular weight component in addition to the primary peak from the monomer transferrin (MW 80,000). The static nature of this distribution was demonstrated by reelution of the two components. The resultant elution profiles are shown in Fig. A.1 (B and C). There is no evidence of an equilibrium between the two components.

The proportion of protein corresponding to the high molecular weight portion ranged between 6 and 15% for three trials. The past history of these three samples (i.e whether or not they were from the same lot #) is not known. These proportions were approximated by the cut-and-weigh method of determining peak areas.

The high molecular weight fraction binds iron quantitatively. This was demonstrated by saturating the protein fraction with iron and measuring the absorbance at 465 nm. This component was then concentrated from 1.3 mL to approximately 0.3 mL by ultrafiltration. Fig. A.2 shows the EPR spectrum of this sample; it is indistinguishable from

the EPR spectrum of normal transferrin.

An SDS-PAGE (sodium dodecyl sulfate- polyacrylamide gel electrophoresis) experiment, which separates proteins approximately according to their molecular weights, was performed on the high molecular weight component. (See Section II for experimental details.) The fraction separated into three proteins, one of which migrated like monomeric transferrin. If we assume that the intermediate component is a dimer, it is possible to make a plot of the log of the molecular weight as a function of relative mobility. This plot is shown in Fig. A.3. From the mobility value of the third peak, we estimate its molecular weight to be 229,000, which would mean it is most likely a trimer. Unfortunately, the standards run with the SDS-PAGE experiment did not appear on the developed gel. A solubility problem may be the reason for this. Clearly, more definitive conclusions concerning the molecular weights of the components await further study.

It is likely that the aggregates are a result of the lyophilization step used in the protein preparation. Huggins (81) first suggested a mechanism for the cross-linking reaction leading to protein aggregation:

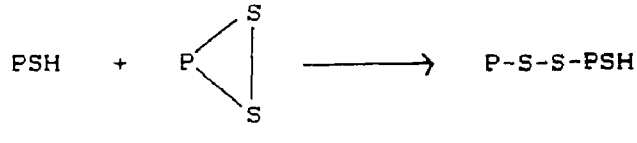

where P denotes interacting protein molecules. Disulfide bonds in proteins can be reduced under relatively mild

conditions (82) and it is known that some commercial preparations of transferrin contain a reducing agent (83). By increasing the concentration of reactants, the process of lyophilization is expected to promote the cross-linking reaction.

The EPR spectrum of the high molecular weight component, as well as the quantitative bonding of iron by the protein, indicate that the iron binding properties of the protein are unaffected by aggregation. Thus, for most studies on the iron binding properties of the protein, it is unlikely that the presence of the high molecular weight component presents a problem.

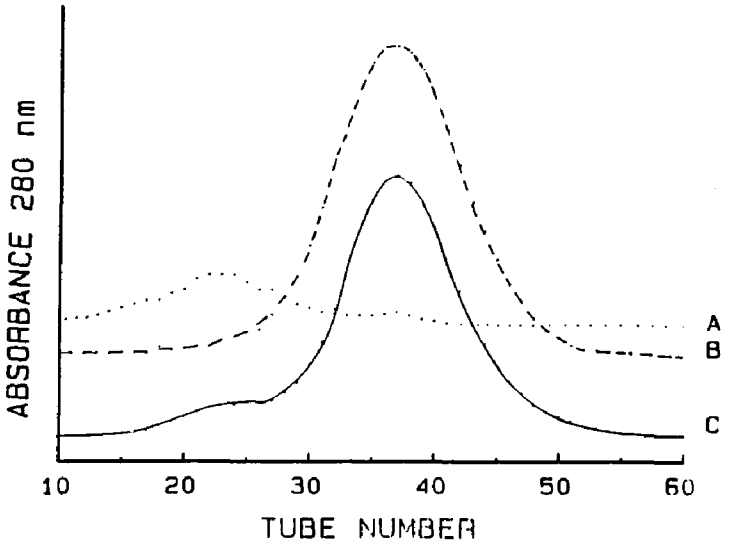

Figure A.1 Elutions profiles of apotransferrin from a Sephadex-200 column. A is the high molecular weight component from C, concentrated by ultrafiltration and re-eluted on the column; B is the main peak from C, concentrated and re-eluted as for B. Samples were dissolved in 10 mM ammonium bicarbonate; sample size for C is 2 mL of 0.042 mM apotransferrin. Samples A and B were 1 mL of unknown concentration, concentrated by ultrafiltration. Column dimensions: 1.5 cm inner diameter, approximately 70 cm long, flow rate approximately 0.16 mL/min. Files 41284D, 41284M and 4884B, disc 6-86.

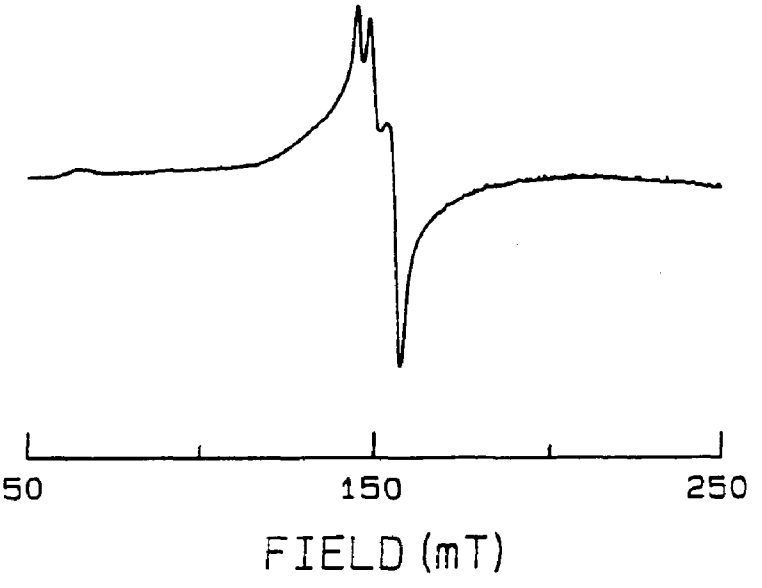

Figure A.2 EPR spectrum of the high molecular weight fraction saturated to 100% with iron. Solution conditions: 100 mM Hepes, 20 mM sodium bicarbonate, 0.06 mM protein, pH 7.4. Instrument settings: field set = 150 milliTesla, scan range = 2000 milliTesla, time constant = 1 s, scan time = 16 min/2000 milliTesla, molulation amplitude = 10 milliTesla, receiver gain = 2500, temperature = 77K, microwave power = 20 milliwatts, microwave frequency = 9.149. File HMW.2K, disc #5.

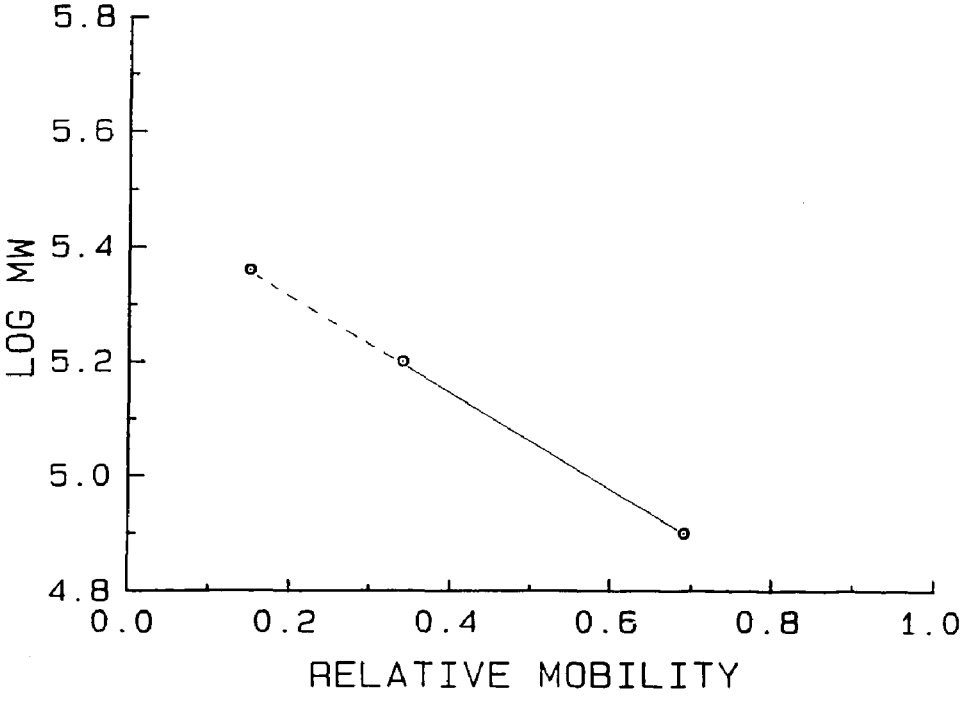

Figure A.3 The log of the molecular weight as a function of the relative mobility of the high molecular weight components for SDS-PAGE. File SDSMW, disc 6-86.

SECTION II: EXPERIMENTAL PROCEDURE FOR SODIUM DODECYL SULFATE POLYACRYLAMIDE GEL ELECTROPHORESIS

This procedure is taken from the laboratory of Dr. J. Williams, The University of Bristol, Bristol, England.

The following two stock solutions are made and refrigerated. The loading solution freezes at normal refrigerator temperatures:

Stock Buffer: 48.4 g tris (base), 16.4 g sodium acetate, 7.4 g EDTA, pH 7.4 adjusted with glacial acetic acid (15-20 ml), in 1 L.

Sample Loading Solution: 5 g SDS (sodium dodecyl sulfate, sodium lauryl sulfate), 14 mL glycerol, 10 mg bromthymol blue, 186 mg EDTA, 2 mL 1M tris, pH 8, 1% mercaptoethanol if desired in 100 mL total.

The day of the experiment, the following is done:

1. Make **Tank Buffer**: Dissolve 1 g SDS in 800 mL H_2O by boiling. Add 100 mL **Stock Buffer** and 100 mL H_2O.

2. Make the gel: Dissolve 3.75 g acrylamide, 0.100 g bisacrylamide, and 30 mg sodium persulfate in 50 mL of Tank Buffer. Add 45 uL of TEMED (N,N,N'N'-tetramethyl ethylenediamine) to the cooled acrylamide solution, stirring slowly without causing frothing. Pour the gel. It requires approximately 1 hour to set.

3. Prepare the sample: 50 uL of sample from fraction collector tube is added to 100 uL of Loading Solution. Samples are then boiled for approximately 3 min. Approximately 20 uL of sample is loaded on a 24 slot gel. Pure transferrin is run as a marker.

4. Electrophoresis: Fill the tank with the Tank Buffer. Electrophorese at 120 V for 3 hr. Stain for 1/2 hr.

REFERENCES

REFERENCES

1. Huheey, J.E. Inorganic Chemistry; Harper and Row: New York, 1978; p 763.

2. Bezkorovainy, Anatoly. Biochemistry of Non-Heme Iron, Plenum: New York, 1980; p 5.

3. Chasteen, N.D. Coord. Chem. Rev. 1977, 22, 1-36.

4. Harris, D.C.; Aisen, P. In Advances in Inorganic Biochemistry; Eichhorn, G.L.; Marzilli, L.G., Eds.; Elsevier: New York, 1986; Vol. 8.

5. Crichton, R.R. In Proteins of Iron Storage and Transport; Spik, G.; Montreuil, J.; Crichton, R.R.; Mazurier, J., Eds.; Elsevier: Amsterdam, 1985; pp 99-110.

6. Katz, J.H. J. Clin. Invest. 1961, 40, 2143-2692.

7. MacGillivray, R.T.A.; Mendez, E.; Sinha, S.K.; Sutton, M.R.; Lineback-Zins, J.; Brew, K. Proc. Natl. Acad. Sci. USA 1982, 79, 2504-2508.

8. Metz-Boutigue, M.H.; Jolles, J.; Mazurier, J.; Schoentzen, F.; Legrand, D.; Spik, G.; Montreuil, J.; Jolles, P.; Eur. J. Biochem. 1984, 145, 659-676.

9. Williams, J.; Elleman, T.C.; Kingston, I.B.; Wilkins, A.G.; Kuhn, K.A. Eur. J. Biochem. 1982 122,. 297-303.

10. Jeltsch, J.M.; Chambon, P. Eur. J. Biochem. 1982, 122, 291-295.

11. Garratt, R.; Lindley, P.; Evans, R.; Hasnain, S. In Proteins of Iron Storage and Transport; Spik, G.; Nontreuil, J.; Crichton, R.R.; Mazurier, J., Eds.; Elsevier: Amsterdam, 1985; p 57.

12. Gorinsky, B.; Horsburgh, C.; Lindley, P.F.; Moss, D.S.; Parkar, M.; Watson, J.L. Nature 1979, 281, 157-158.

13. Chasteen, N.D. Trends Biochem. Sci. 1983, 8, 272-275.

14. Montreuil, J.; Mazurier, J.; Legrand, D.; Spik, G. In Proteins of Iron Storage and Transport Spik, G.; Montreuil, J.; Crichton, R.R.; Mazurier, J., Eds.; Elsevier: Amsterdam, 1985; pp 25-38.

15. Williams, J.; Grace, S.A.; Williams, J.M. Biochem. J. 1982, 201, 417-419.

16. Leibman, A.; Aisen, P. Blood 1979, 53, 1058-1065.

17. Zak, O.; Aisen, P. In Proteins of Iron Storage and Transport Spik, G.; Montreuil, J.; Crichton, R.R.; Mazurier, J., Eds.; Elsevier: Amsterdam, 1985, pp 61-64.

18. Princiotto, J.V.; Zapolski, E.J. Nature 1975, 255, 87-88.

19. Makey, D.G.; Seal, U.S. Biochim. Biophys. Acta 1976, 458, 250-256.

20. Williams, J.; Moreton, K. Biochem. J. 1980, 185, 483-488.

21. Williams, J.; Chasteen, N.D.; Moreton, K. Biochem. J. 1982, 201, 527-532.

22. Baldwin, D.A.; DeSousa, D.M.R. Biochim. Biophys. Res. Comm. 1981, 99, 1101-1107.

23. Record, M.T.; Anderson, C.F.; Lohman, T.M. Quart. Rev. Biophys. 1978, 2, 103-178.

24. C.K. Luk. Biochemistry 1971, 10, 2838-2843.

25. Pecoraro, V.L.; Harris, W.R.; Carrano, C.J.; Raymond, K.N. Biochemistry 1981, 20, 7033-7039.

26. Aasa, R.; Malmstrom, B.G.; Saltman, P.; Vanngard, T. Biochim. Biophys. Acta 1963, 75, 203-222.

27. Gaber, B.P.; Miskowski, V.; Spiro, T.G. J. Am. Chem. Soc. 1974, 96, 6868-6873.

28. Chasteen, N.D. In Iron Binding Proteins Without Cofactors or Sulfur Clusters; Theil, E.C.; Eichorn, G.I.; Margilli, L.G., Eds.; Adv. Inorg. Biochem.; Elsevier: New York, 1983; Vol. 5, pp 202-235.

29. Pinkowitz, R.; Aisen, P. J. Biol. Chem. 1972, 247, 7830-7834.

30. Schlabach, M.R.; Bates, G.R. J. Biol. Chem. 1975,250, 2182-2188.

31. Aisen, P.; Pinkowitz, R.A.; Liebman, A. Ann. N.Y. Acad. Sci. 1973, 222, 337-346.

32. Price, E.M.; Gibson, J. J. Biol. Chem. 1972, 247, 8031-8035.

33. Folajtar, D.A.; Chasteen, N.D. J. Am. Chem. Soc. 1982, 104, 5775-5780.

34. Thompson, C.P.; McCarty, B.M.; Chasteen, N.D. Biochim. Biophys. Acta 1986, 870, 530-537.

35. Aisen, P. In Iron Metabolism, Ciba Foundation Symposium; Elsevier: Amsterdam, 1977; p 1.

36. Cowart, R.E.; Kojima, N.; Bates, G.W. J. Biol. Chem. 1982, 257, 7560-7565.

37. Cowart, R.E.; Swope, S.; Loh, T.T.; Chasteen, N.D.; Bates, G.W. J. Biol. Chem. 1986, 261, 4607-4614.

38. Pollack, S.; Vanderhodd, G.; Lasky, G. Biochim. Biophys. Acta 1977, 497, 481-487.

39. Morgan, E.H. Biochim. Biophys. Acta 1977, 499, 169-177.

40. Folajtar, D. Ph.D. Thesis. University of New Hampshire, Durham, New Hampshire, 1982.

41. Cannon, J.C.; Chasteen, N.D. Biochemistry 1975, 14, 4573-4577.

42. Baldwin, D.A.; deSousa, D.M.R.; Ford, G. In The Biochemistry and Physiology of Iron; Saltman, P.; Hegenauer, J., Eds.; Elsevier: New York, 1982; p 57.

43. Chasteen, N.D. The University of New Hampshire, personal communication, 1986.

44. Geoghegan, K.F.; Dallas, J.L.; Feeney, R.E. J. Biol. Chem. 1980, 255, 11429-11434.

45. Rosseneu-Metreff, M.Y.; Soetewy, F.; Lamote, R.; Peters, H. Biopolymers 1971, 10, 1039-1048.

46. Baldwin, D.A.; DeSousa, D.M.R.; van Wandruszka, R.M.A. Biochim. Biophys. Acta 1982, 719, 140-146.

47. Ehrenberg, A.; Laurell, C.B. Acta. Chem. Scand. 1955, 9, 68-72.

48. Windle, J.J.; Wiersema, A.K.; Clark, J.R.; Feeney, R.E. Biochemistry 1963, 2, 1341-1345.

49. Spartalian, K.; Oosterhuis, W.T. J. Chem. Phys. 1973, 59, 617-622.

50. Tsang, C.P.; Boyle, A.J.F.; Morgan, E.H. Biochim. Biophys. Acta 1973, 328, 84-94.

51. Purcell, K.F.; Kotz, J.C. Inorganic Chemistry; W.B. Saunders: Philadelphia, 1977; p 547.

52. Feltman, R.D.; Silverthorn, W. Inorg. Chem. 1970, 9, 1207-1210.

53. Dunn, T.M.; Nyholm, R.S.; Yamada, S. J. Chem. Soc. 1962, 1564-1566.

54. Tsai, R.; Yu, C.A.; Gunsalus, I.C.; Peisach, J.; Blumberg, W.: Orme-Johnson, W.H.; Beiner, H. Proc. Natl. Acad. Sci. USA 1970, 66, 1157-1163.

55. Fisher, M.T.; Sligar, S.G. J. Am. Chem. Soc. 1985, 107, 5018-5019.

56. Holm, R.H.; Everett, G.W. Jr.; Chakravorty, A. Prog. Inorg. Chem. 1966, 7, 83-214.

57. Daul, C.; Schlapfer, C.W.; von Zelewsky, A. Structure and Bonding 1979, 36, 129-171.

58. Nishida, S.; Oshio, S.; Kida, S. Inorg. Chim. Acta 1977, 23, 59-61.

59. Kotani, M. Supp. Prog. Theoret. Phys. 1961, 17, 4-13.

60. Gibson, J.F.; Ingram, D.J.E. Nature 1957, 180, 29.

61. Griffith, J.S. Nature 1957, 180, 30.

62. LaMar, G.N.; Walker, F.A. J. Am. Chem. Soc. 1973, 95, 1782-1790.

63. Nishida, Y.; Oshio, S.; Kida, S. Chemistry Letters 1975, 79-80.

64. Collman, J.P.; Sorrell, T.N.; Hodgson, K.O.; Kulshrestha, A.K.; Strouse, C.E. J. Am. Chem. Soc. 1977, 99, 5180-5181.

65. Aisen, P.; Aasa, R.; Malmstrom, B.G.; Vanngard, T. J. Biol. Chem. 1967, 242, 2484-2490.

66. Weber, K. B.S. Thesis, University of New Hampshire, Durham, N.H., 1985.

67. Taube, H. Chem. Rev. 1952, 50, 69-126.

68. Gutlich, P. In Mossbauer Spectroscopy and Its Chemical Applications; Comstock, M.J. Ed.; Advances in Chemistry 194; American Chemical Society: Washington, D.C., 1981; p 405.

69. Bates, G.W.; Schlabach, M.R. J. Biol. Chem. 1975, 250, 2177-2181.

70. Springarn, N.E.; Sartorelli, A.E. J. Med. Chem. 1979, 22, 1314-1316.

71. Raina, R.; Srivastava, T.S. Inorg. Chim. Acta. 1984, 91, 137-140.

72. James, T.L. Nuclear Magnetic Resonance in Biochemistry; Academic Press: New York, 1975.

73. Mason, J. Chem. Rev. 1981, 813, 205-227.

74. Levy, G.C.; Lichter, R.L. Nitrogen-15 Nuclear Magnetic Resonance Spectroscopy; Wiley Intersccience: New York, 1979.

75. Martin, M.L.; Martin, G.J. Practical NMR Spectroscopy; Heyden: London, 1980; chapter 7.

76. JEOL; Technical Bulletin NMB-10; February 8, 1977.

77. Koenig, S.H.; Schillinger, W.E. J. Biol. Chem. 1969, 244, 6520-6526.

78. Chasteen, N.D. In Biological Magnetic Resonance, Lawrence, Ed.; Plenum: New York, 1981, p 53.

79. Burton, D.R.; Forsen, S.; Karlstrom, G.; Dwek, R.A. Prog. in NMR Spectroscopy 1979, 13, 1-45.

80. Mildvan, A.S.; Cohn, M. Adv. Enzymology 1970, 33, 1-69.

81. Huggins, C.; Tapley, D.F.; Jensen, E.V. Nature 1951, 167, 592- .

82. Means, G.E.; Feeney, R.E. Chemical Modification of Proteins; Holden-Day: San Francisco, 1971; p 149.

83. Chasteen, N.D.; Grady, J. K.; Holloway, C.E. Inorganic Chemistry 1986 25, 2754-2760.